Review

Glassy Polymers—Diffusion, Sorption, Ageing and Applications

Raj Kumar Arya [1,*] **, Devyani Thapliyal** [1] **, Jyoti Sharma** [2] **and George D. Verros** [3,*]

[1] Department of Chemical Engineering, Dr. B.R. Ambedkar National Institute of Technology, Jalandhar 144011, India; devyanithapliyal5@gmail.com

[2] School of Chemistry and Biochemistry, Thapar Institute of Engineering & Technology, Bhadson Road, Patiala 147004, India; jyotisharma.1328@gmail.com

[3] Laboratory of Chemistry and Technology of Polymers and Colors, Department of Chemistry, Aristotle University of Thessaloniki, P.O. Box 454, Plagiari, 57500 Thessaloniki, Greece

* Correspondence: aryark@nitj.ac.in (R.K.A.); gdverros@yahoo.gr (G.D.V.)

Abstract: For the past few decades, researchers have been intrigued by glassy polymers, which have applications ranging from gas separations to corrosion protection to drug delivery systems. The techniques employed to examine the sorption and diffusion of small molecules in glassy polymers are the subject of this review. Diffusion models in glassy polymers are regulated by Fickian and non-Fickian diffusion, with non-Fickian diffusion being more prevalent. The characteristics of glassy polymers are determined by sorption isotherms, and different models have been proposed in the literature to explain sorption in glassy polymers over the last few years. This review also includes the applications of glassy polymers. Despite having many applications, current researchers still have difficulty in implementing coating challenges due to issues such as physical ageing, brittleness, etc., which are briefly discussed in the review.

Keywords: glassy polymers; diffusion; sorption; physical ageing; polymer coatings; gas-separation membranes

1. Introduction

Polymers are macromolecules which are made up of several smaller components called monomers joined together. Polymers are categorised as amorphous polymers and crystalline polymers based on their morphology. Amorphous polymers are those that have amorphous areas in which molecules are randomly organised. Crystalline polymers have molecules that are evenly packed. All crystalline polymers have 30 amorphous zones; therefore, there is no polymer which is 100% pure crystalline.

Due to their non-uniform packed structure, amorphous polymers do not possess sharp melting points but have a broader range of temperature. They are classified as glassy polymers only when they are in glassy state at room temperature, and have higher glass transition temperature (T_g) than room temperature. However, rubbery polymers and semi-crystalline polymers have a T_g lower than room temperature [1]. Glassy polymers have a non-crystalline structure and high stiffness, which makes them mechanically strong to exist as hollow fibre membranes or porous flat films. The mechanical properties of coatings are important, including adhesive strength, fracture toughness, tensile and compressive strength, and wear resistance.

The atoms or molecules in glassy polymers are not arranged in a regular pattern. Bulky constituents, rigid main chains, and low cohesive energies result in a high free volume. From the last decade, the study of glass transition temperatures and viscoelastic properties of glassy polymers has been the subject of much research. Examples of some common amorphous glassy polymers include polystyrene, polyvinyl acetate, polylactic acid, polyvinyl chloride, polymethyl methacrylate, polysulfone, poly(ether sulfone), polyimide, polycarbonate, etc.

Polylactic acid has been investigated as a potential future substitute for common plastics in a number of applications, including food packaging and medical implants [2,3]. Poly(1-trimethylsilyl-1-propyne) is frequently employed in gas permeable membranes because of its excellent permeability to low-molecular-weight organic gases and vapours [4,5]. Polyacrylamide can be utilised in drug delivery systems as a hydrogel [6]. Poly (4-methyl-2-pentyne) is employed in the separation of methane and n-butane [7]. Budd et al. [8] described a novel family of polymers of intrinsic microporosity for application in gas-separation membranes. These materials feature twisted ladder-like backbones made up of spiro-centres and stiff fused dioxane rings, which prevent the high free volume structure from relaxing.

In comparison to rubbery polymers, glassy polymers have greater solubility coefficients and a lower diffusion coefficient. Additionally, almost all glassy polymers have permselectivity values around or at the upper bound. Rubbery polymers have a higher diffusivity selectivity than glassy polymers as a result [9]. These polymers can be transformed into rubbery states either by raising the temperature above glass transition, or the addition of solvent(s) or other additives.

Films of glassy polymers are prepared by using their rubbery solutions. Glassy films are initially coated from solvent solutions followed by drying in natural convection, forced convection or in industrial dryers. The choice of drying conditions such as air flow rate, air temperature, and solvent humidity control the film formation, quality, drying time, etc. The polymer is dissolved in sufficient solvent; therefore, the coating is initially rubbery due to the presence of high amounts of solvent. During the course of drying, the rubbery solution changes to glassy as soon as the solvent level drops down below the critical solvent mass fraction which is required for transition [10]. When processing temperatures are low enough, the rubbery state transforms into a glassy transition, and during the early stages of drying, as concentration gradients grow within the film, a rubbery–glassy transition forms at the coating–gas interface, creating a glassy skin. This glassy skin grows with respect to time due to more and more solvent removal from the coating. Ultimately, the entire film turns into glassy state.

In this article, a brief overview of glassy polymer modelling, as well as theories and factors that influence their properties with their limitations and applications are presented in order to direct future research to find suitable models for the prediction of data. The work performed over the last decade is highlighted. Figure 1 shows the brief main topics covered in this review.
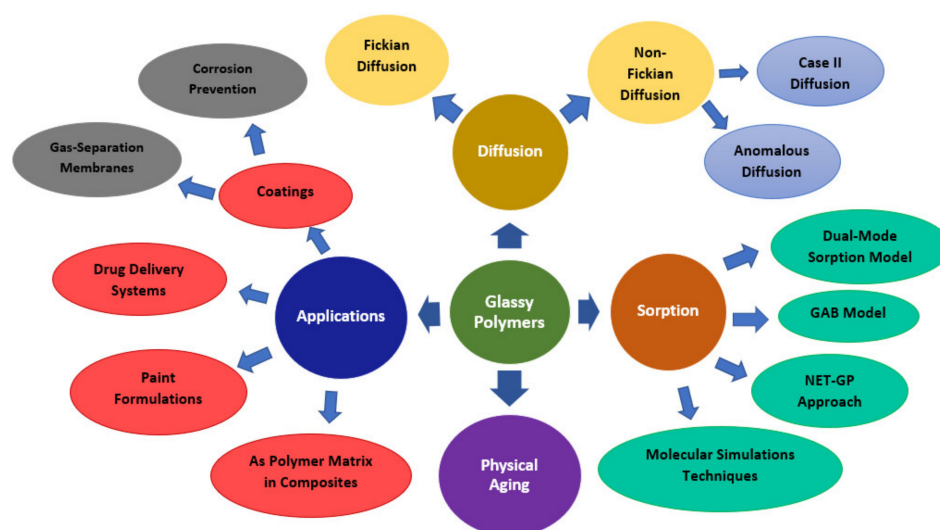

Figure 1. Graphical representation of an overview of the contents of the present review.

2. Diffusion in Glassy Polymer Systems

The diffusion of small molecules in glassy polymers is essential in practice and has been widely studied. Above the glass transition temperature of the pure polymer, diffusion is reliably predictable over a wide range of temperatures and concentrations. Free volume in the polymer is described as the volume of the total mass which is not occupied by polymer chains so that diffusing molecules can fit in it. Solvents increase the free volume in the polymer, and diffusion in the free volume polymer chains. The transport phenomenon is controlled by diffusion. Theories based on diffusion and free volume help in predicting and correlating the self-diffusion of solvents and polymers in the rubbery polymer–solvent systems [11,12].

The transport phenomenon of drying is generally governed by Fick's first law of diffusion. According to this law, the flux of a particular component is equal to the diffusion coefficient times the concentration gradient. The rate of change in concentration with time is given by Fick's second law of diffusion:

$$\frac{\partial c}{\partial t} = \frac{\partial}{\partial z}\left(D\frac{\partial c}{\partial z}\right)$$

(1)

where c is the concentration (g/cm^3), D is the mutual diffusion coefficient (cm^2/s), t is the time (s), and z is the distance (cm).

The self-diffusion coefficients are calculated using free volume theory. This theory is applicable for polymer–solvent coatings [13–19], and the extension of this theory to polymer–solvent–solvent systems has also been reported [20,21]. The self-diffusion coefficient in a ternary polymeric system is given by:

$$D_i = D_{0i}\ \exp\left(-\frac{\left(\sum\limits_{j=1}^{3}\omega_j \hat{V}_j^* \frac{\xi_{i3}}{\xi_{j3}}\right)}{\frac{\hat{V}_{FH}}{\gamma}}\right)$$

(2)

where V_j^* is the specific critical hole-free volume of a component of j, ω_j is the mass fraction of the component j, D_{0i} is the pre-exponential factor, γ is the overlap factor, ξ is the ratio of molar volumes of the solvent and the polymer jumping units, and $\frac{\hat{V}_{FH}}{\gamma}$ is the free-volume parameter.

There are two distinct points of view given in the literature in relation to the free volume and corresponding mechanisms for diffusion and sorption in the glassy state. Both points are agreed in that when a polymer reaches the glassy state, the excess free volume is incorporated, or at least temporarily frozen, into the matrix.

Glassy state in the polymer solutions refers to when polymer solutions are cooled over practical time scales and the rate of cooling exceeds the rate of relaxation of the polymer. This phenomenon causes volume to be trapped in the polymer in excess of that expected at equilibrium. Free-volume theory presumes that this extra volume is available to facilitate mass transport in the glassy state.

On the other hand, in rubbery coatings, there is no volume change on mixing, and the modelling analysis is greatly simplified by using the volume-average velocity. In glassy polymer solutions, however, the addition or removal of solvents leads to structural rearrangements in the polymer matrix as it gradually moves toward a denser equilibrium liquid configuration during sorption or toward an unrelaxed glassy state during desorption/drying.

If the polymer is a rubber, i.e., the sorption temperature is higher than the glass transition temperature of the polymer, it behaves in a liquid-like manner and the penetrant (gas) concentrations in the polymer can be described by Henry's law [22]. Cooling down a polymer from the rubbery state, it undergoes a gradual change in its properties at the glass

transition temperature. Additionally, to the liquid free volume, there is the unrelaxed free volume moieties frozen into the matrix, available for sorption.

Different models of diffusion in glassy polymer coatings are developed by a variety of theories. They are classified using the following formula: $M_t = kt^n$, where M_t is the absorbed per unit area of polymer after an elapsed time t, and k is a constant. Fickian diffusion is recognised when the exponent $n = 1/2$; Case II diffusion is known when $n = 1$; and anomalous diffusion is recognised when $1/2 < n < 1$ [23]. Case II diffusion and anomalous diffusion come under non-Fickian diffusion.

The diffusion kinetics are called Fickian if the solvent transport inside the film is exclusively regulated by diffusion. Fickian diffusion models can reliably predict the drying rate for the initial drying time, whereas visco-elastic models can predict the solvent concentration profiles. By fitting the initial drying rate to pure Fickian diffusion, one may reliably predict the polymer–solvent diffusion coefficient. Using systematic experimental methods such as confocal Raman spectroscopy, it has been shown in the literature that there is an increased solvent concentration region well away from the drying surface.

Non-Fickian diffusion processes are most commonly found in glassy polymers at temperatures below T_g. The polymer chains are not sufficiently mobile at temperatures below T_g to allow the solvent to penetrate the polymer core immediately [24]. The fundamental distinction between Case II diffusion and anomalous diffusion is the rate of solvent diffusion. The solvent diffusion rate is more rapid than the polymer relaxation process in Case II diffusion, whereas the solvent diffusion rate and polymer relaxation rate are comparable in anomalous diffusion. In general, when solvents have high activity, Case II diffusion occurs [25].

Vrentas and Vrentas [26] described the free-volume fluctuations in glassy polymers produced by the presence of a small molecule. They suggested a model based on the idea that the penetrant concentration varies with the molecular structure of glassy polymer. The notion that the molecular structure of the glassy polymer differs at each concentration causes $\hat{V}_{2g}^0$ to be concentration-dependent. The equation gives a volume expansion which is fairly consistent with the experimental data:

$$\frac{V_m}{V_0} = \frac{\frac{\omega_1}{1-\omega_1}\hat{V}_1^0 + \hat{V}_{2y}^0(\omega_1)}{\hat{V}_{2y}^0(\omega_1 = 0)} \tag{3}$$

where

$$\hat{V}_{2g}^0(\omega_1) = \hat{V}_2^0(T_{gm})\left[1 + \alpha_{2g}(T - T_{gm})\right] \tag{4}$$

$\hat{V}_{2g}^0$ is the appropriate specific volume of the glassy polymer at penetrant mass fraction ω_1 temperature T, $\hat{V}_2^0(T_{gm})$ is the specific volume of the equilibrium liquid polymer at T_{gm}, and α_{2g} is the thermal expansion coefficient calculated when a pure polymer is cooled below T_{g2}. This relationship is given by Vrentas and Duda [27]. The glass transition temperature of the polymer–penetrant mixture, T_{gm}, is given by:

$$T_{gm} = T_{g2} - A\omega_1 \tag{5}$$

where coefficient A is determined by the type of penetrant employed to lower a polymer's glass transition temperature T_{g2}.

They highlighted that predicting the volumetric behaviour for glassy polymer–penetrant systems is more challenging when the penetrant is a gas rather than a liquid at the temperature of interest, because a reasonable estimate for constant specific volume, $\hat{V}_1^0$, is often unavailable for gaseous penetrants.

Laksmana et al. [28] predicted diffusion coefficients of glassy polymers based on the estimation methods of the polymer fractional free volume at different environmental conditions using the model of Vrentas and Duda [27]. Moisture sorption and T_g values were measured on different hydroxypropyl methylcellulose free films with varying water activities. Moisture content, storage temperature, and the molecular weight of the polymer

were found to influence the fractional free volume of the films. The researchers determined a relationship between the diffusion coefficient of moisture via films and fractional free volume, enabling the computation of diffusion coefficients of moisture via films under various environmental conditions.

The mutual diffusion coefficient for a given solvent–polymer system is frequently the most basic physical property needed to design and optimise polymer processing operations as well as other polymer products. Duda et al. [29] gave the most concise way to describe the effect of anti-plasticization and molecular diffusion on gas permeation by using free volume models. The concept of free volume is used to explain molecular motion in liquids and solids. To test the free-volume hypothesis, they employed inverse gas chromatography technique with a capillary column coated with a polymer film to present experimental measurements of toluene diffusion in polystyrene above and below the T_g. The effect of temperature on diffusivity for a solvent–polymer system above and below the T_g was demonstrated to be compatible with the free-volume formulation provided in Equation (7). They modified the Vrentas–Duda [30] free-volume model for diffusion above the T_g to describe the diffusion of low-molecular-weight species in glassy polymers. As the solvent concentration tends to zero, the solvent self-diffusion coefficient becomes equal to the binary mutual diffusion coefficient and is given by:

$$
\begin{aligned}
D = D_1 &= D_{01} \exp\left[-y\xi \hat{V}_2^* / \hat{V}_{FH_2}^*\right], \\
\frac{\hat{V}_{FH_2}^g}{\gamma} &= \frac{K_{12}}{\gamma}\left[K_{22} + \lambda\left[T - T_{g2}\right]\right], \\
\lambda &= 1 - \hat{V}_2^0\left(T_{g2}\right)\left(\alpha_{2-}\alpha_{2g}\right) / K_{12}
\end{aligned}
\tag{6}
$$

where K_{12} and K_{22} are related to the free-volume characteristics of the polymer, λ is related to the change in the expansion coefficient of the polymer above T_g, α_2 and the expansion coefficient of the glassy polymer, α_{2g}, and $\hat{V}_2^0\left(T_{g2}\right)$ is the volume of the polymer at T_{g2}.

Wang et al. [31] also used free volume theory to propose a model for predicting solvent self-diffusion coefficients in amorphous glassy polymers. This new model takes into account the plasticization effects caused by small molecular solvents to correctly estimate the hole-free volume variance above and below T_g. To express the plasticization effect, only one parameter is added, and it can be easily calculated using thermodynamic theory about the glass-transition temperature depression. For benzene–polystyrene mixtures, the authors discovered that the hole-free volume decreases as the temperature drops. The hole-free volume of a mixture with a higher solvent concentration is often greater than that of a mixture with a lower concentration, according to the findings. The estimated hole-free volume is higher than that calculated using the original and updated theories, resulting in a higher diffusion coefficient in this analysis.

For toluene-poly(methyl methacrylate) films, Verros [32] presented a model for solvent–polymer mutual diffusion coefficients in the glassy state. Irreversible thermodynamics serve as the foundation for this paradigm. The gravimetric data of Powers and Collier [33] were used to test the theory proposed in this study. This idea is a precise application of Fick's law that does not include the relaxation time component. This was accomplished by including relaxation time effects in chemical potential terms through proper transformation. This allowed existing equations to be used for the glassy state to compute mutual diffusion coefficient in rubbery state as a function of solvent self-diffusion coefficient and chemical potential. Figure 2a shows that the results were in agreement with the experimental data. Figure 2b shows the volume fraction profiles of toluene at various evaporation times. The Galerkin Finite Element technique [34] was used to solve the model equations at the same time. The findings of this research might be used to study diffusion in the amorphous glassy state.
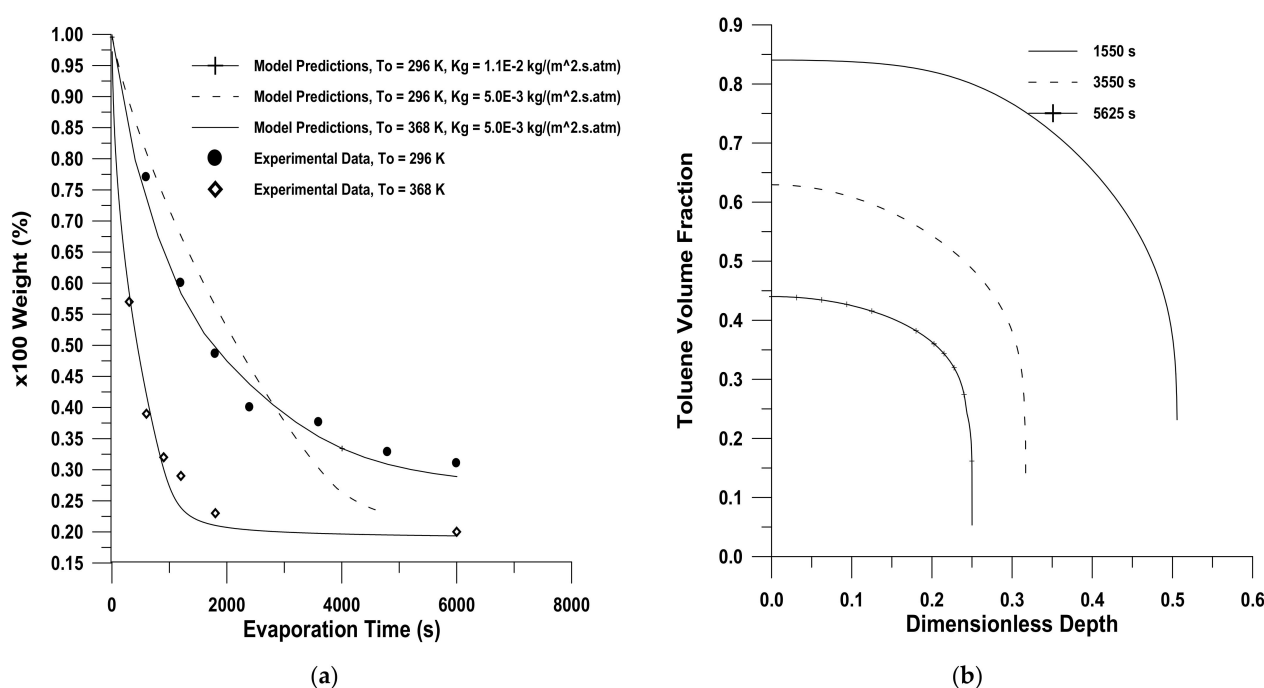
Figure 2. Fickian diffusion for the system poly(methyl methacrylate)/toluene (used with copyright permission) [32].
(**a**) Polymeric coating mass versus drying time for various drying temperatures. Initial coating thickness = 2 mm; (x_∞ = 0).
(**b**) Toluene volume fraction profiles for different drying times. Drying air = 296 K; Initial coating thickness = 2 mm; (x_∞ = 0).

Sharma et al. [35], our research group, studied the solvent evaporation from the poly(methyl methacrylate)/ethyl benzene method as a one-dimensional numerical moving boundary experiment with simultaneous heat and mass transfer. By considering visco-elastic contribution to diffusion at the later stage of drying, the established model follows non-equilibrium thermodynamics principles. To solve the model equations, they used the Galerkin finite element method [34]. They used the Alsoy and Duda model [36] to estimate the ethyl benzene mutual diffusion coefficient in the rubbery state ($T \geq T_{gm}$):

$$D = \frac{D_1 u_1}{RT} \frac{\partial \mu_1}{\partial u_1} \; ; \; T \; < \; T_{gm} \tag{7}$$

Figure 3 shows the solution weight fraction with time in a poly(methyl methacrylate)/ethyl benzene system, in which the results showed that the model was under-predicting in the beginning and over-predicting afterwards. However, there is good fit between solvent weight fraction with depth, as shown in Figure 4.

Sharma et al. [37] also developed a detailed model for the drying of glassy polymeric coatings by observing the evaporation of thin films of poly(styrene)/p-xylene solutions. The proposed model considers Fickian diffusion at high solvent concentrations. The model also considered visco-elastic contributions to diffusion towards the end of the drying process. The drying rate and concentration profiles predicted by the model were found to be in good agreement with the available data, as shown in Figure 5.

SEM analysis of the final coating, which revealed a one-phase system with no bulk flows within the film, further validated the assumptions made in this study, as shown in Figure 6. A 1D numerical experiment was used to investigate the drying of the poly(styrene)-p-xylene coating.
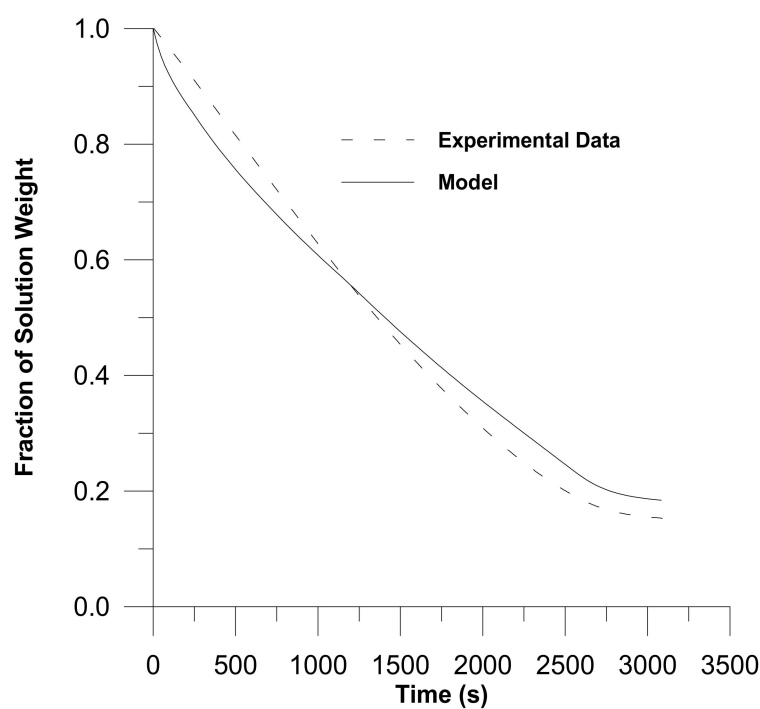
Figure 3. Non-Fickian diffusion for the system poly(methyl methacrylate)/ethyl benzene. Fraction of solution weight as a function of evaporation time. Initial ethyl benzene weight fraction: 0.9014, drying air = 298 K, initial coating thickness = 0.426 mm (used with copyright permission) [35].
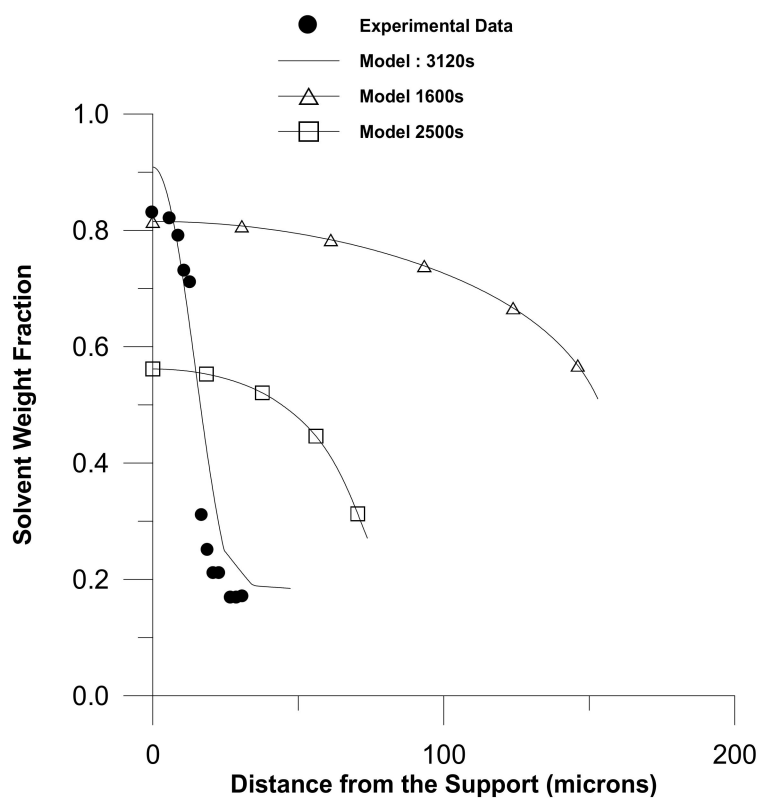

Figure 4. Non-Fickian diffusion for the system poly(methyl methacrylate)/ethyl benzene. Ethyl benzene weight fraction profiles. Initial ethyl benzene weight fraction: 0.9014, drying air = 298 K, initial coating thickness = 0.426 mm (used with copyright permission) [35].
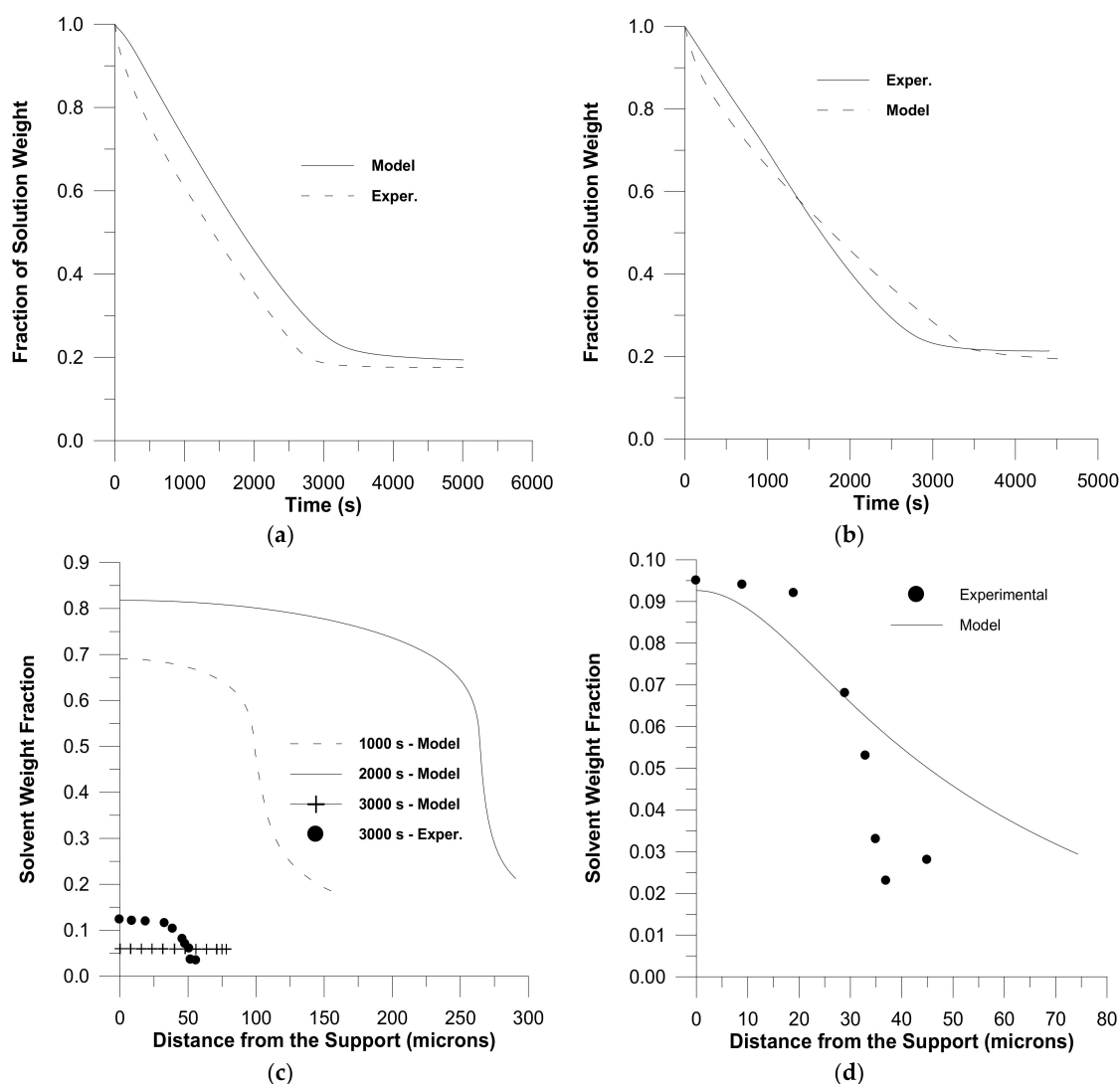
Figure 5. Non-Fickian diffusion for the system poly(styrene)/p-xylene (used with copyright permission) [37]. (**a**) Fraction of solution weight as a function of evaporation time. Initial p-xylene weight fraction: 0.84, drying air = 302 K, initial coating thickness = 0.487 mm. (**b**) Fraction of solution weight as a function of evaporation time. Initial p-xylene weight fraction: 0.84, drying air = 302 K, initial coating thickness = 0.466 mm. (**c**) Solvent weight fraction profiles. Initial p-xylene weight fraction: 0.84, drying air = 302 K, initial coating thickness = 0.487 mm. (**d**) Solvent weight fraction profiles. Initial p-xylene weight fraction: 0.84, drying air = 302 K, initial coating thickness = 0.466 mm.

Davis et al. [38] measured the diffusion of water in polylactide using three methods: quartz spring microbalance, quartz crystal microbalance, and time-resolved Fourier-transform infrared–attenuated total reflectance (FTIR-ATR) spectroscopy in polylactide at various external water vapor activities (0−0.85) and temperatures (25, 35, and 45 °C). They observed non-Fickian sorption kinetic behaviour in all three, which was attributed to the glassy polymer's non-equilibrium state. This non-Fickian behaviour was caused by the glassy polymer's non-equilibrium state, where two-stage sorption kinetics were observed. By regressing the early time data to a Fickian model and the data over the entire observed experimental time scale to a diffusion–relaxation model, they calculated diffusion coefficients and relaxation time constants. The observed that diffusion coefficients from all three experimental methods were equivalent at all temperatures and activities studied, whereas the relaxation time constants varied. The variation in the relaxation time constants may be a product of the different constraints on the polymer film for the different experimental

techniques. The high Deborah numbers (relaxation time/diffusion time) determined from the diffusion–relaxation model confirm the observed two-stage non-Fickian behaviour.
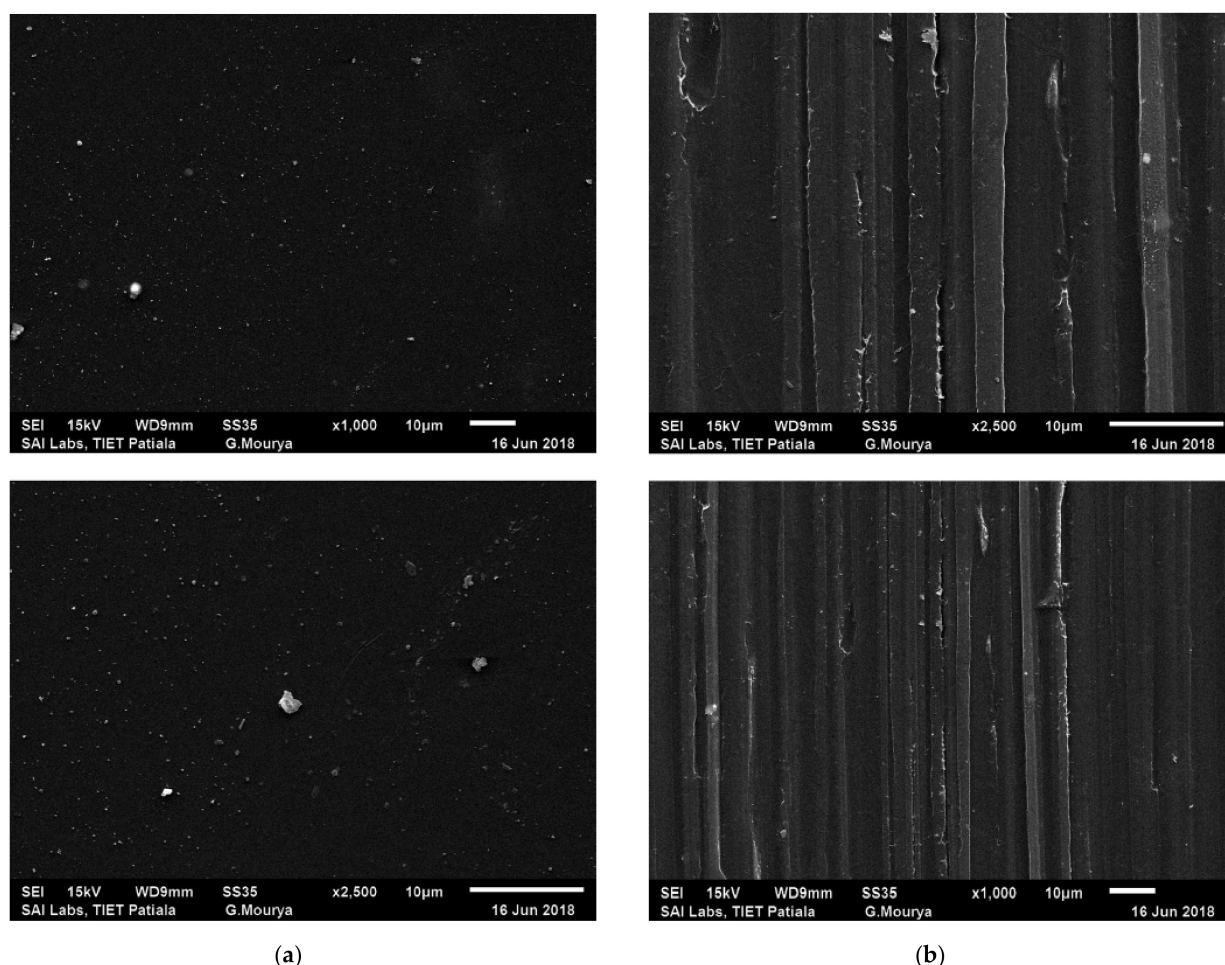
(**a**)　　　　　　　　　　　　　　　　　　　　　　　　(**b**)

Figure 6. The top and bottom surface SEM images of poly(styrene)-p-xylene coatings are shown in (**a**,**b**), respectively. The films appear to be symmetrical, thick, and macroscopically non-porous based on these pictures. No macropores were found in the final coating; therefore, this is a strong indicator of a one-phase system with no bulk flows during drying (used with copyright permission) [37]. (**a**) Top surface SEM images of poly(polystyrene)/p-xylene. Coatings had an initial solvent weight fraction = 0.84, initial coating thickness = 487 microns, T_0 = 303 K, and t = 3000 s. (**b**) SEM images of the substrate side of poly(polystyrene)/p-xylene coatings. Initial solvent weight fraction = 0.84, initial coating thickness = 487 microns, T_0 = 303 K, and t = 3000 s.

Using confocal Raman micro-spectroscopy, Tomba et al. [39] investigated diffusion between a sequence of liquid polystyrenes and a glassy poly(phenylene oxide) matrix. Polystyrene concentration profiles were calculated as a function of molecular weight, diffusion temperature, and annealing time using this model. When the induced stress effectively overcame the glassy matrix's deformation resistance, Case II diffusion occurred. The authors, on the other hand, found no indications of the linear regime that characterised Case II. The fact that a model designed for liquid–liquid polymer diffusion thoroughly explained all diffusion experiments, on the other hand, indicated a Fickian diffusion control mechanism. Based on the findings, the liquid molecular weight appears to affect diffusion rates through free volume effects, which are demonstrated by the diffusion model based on liquid dynamics.

To understand the formation of propagating sharp diffusion fronts, Gallyamov et al. [40] proposed a diffusion model by introducing the strong asymmetry of probability hypotheses for binding/unbinding processes. Plasticisation, unlike in standard Case II models, was not

found to be the driving force for the development of sharp diffusion fronts. The diffusion front, according to the authors, was not a conventional border between glassy and plasticized regions, but rather a site of efficient immobilisation of free diffusant molecules. The model appeared to be very general, and it appears to apply not only to polymers, but also to diffusion in microporous media. The probabilities for macromolecules to be captured by unique sites of a polymer matrix and then released are taken into account in the diffusion with changes in the state model.

Santos et al. [41] also used in situ pressure-contact FTIR-ATR spectroscopy to measure liquid transport in free-standing polymer films. They investigated liquid water transport in free-standing films of a rubbery polymer–poly(isobutylene), a glassy polymer–poly(methyl methacrylate), and a crosslinked polymer–epoxy/amine resin. The non-Fickian behaviour observed for the rubbery polymer was found to be due to clustering behaviour in water caused by self-associating H-bonding. Due to water diffusion and water-induced polymer relaxation occurring on the same time scale, the glassy polymer also displayed non-Fickian behaviour. The suppression of the polymer strain response was blamed for the Fickian behaviour observed in the crosslinked polymer film. Figure 7 shows the absorbance of water molecules in various polymer systems.
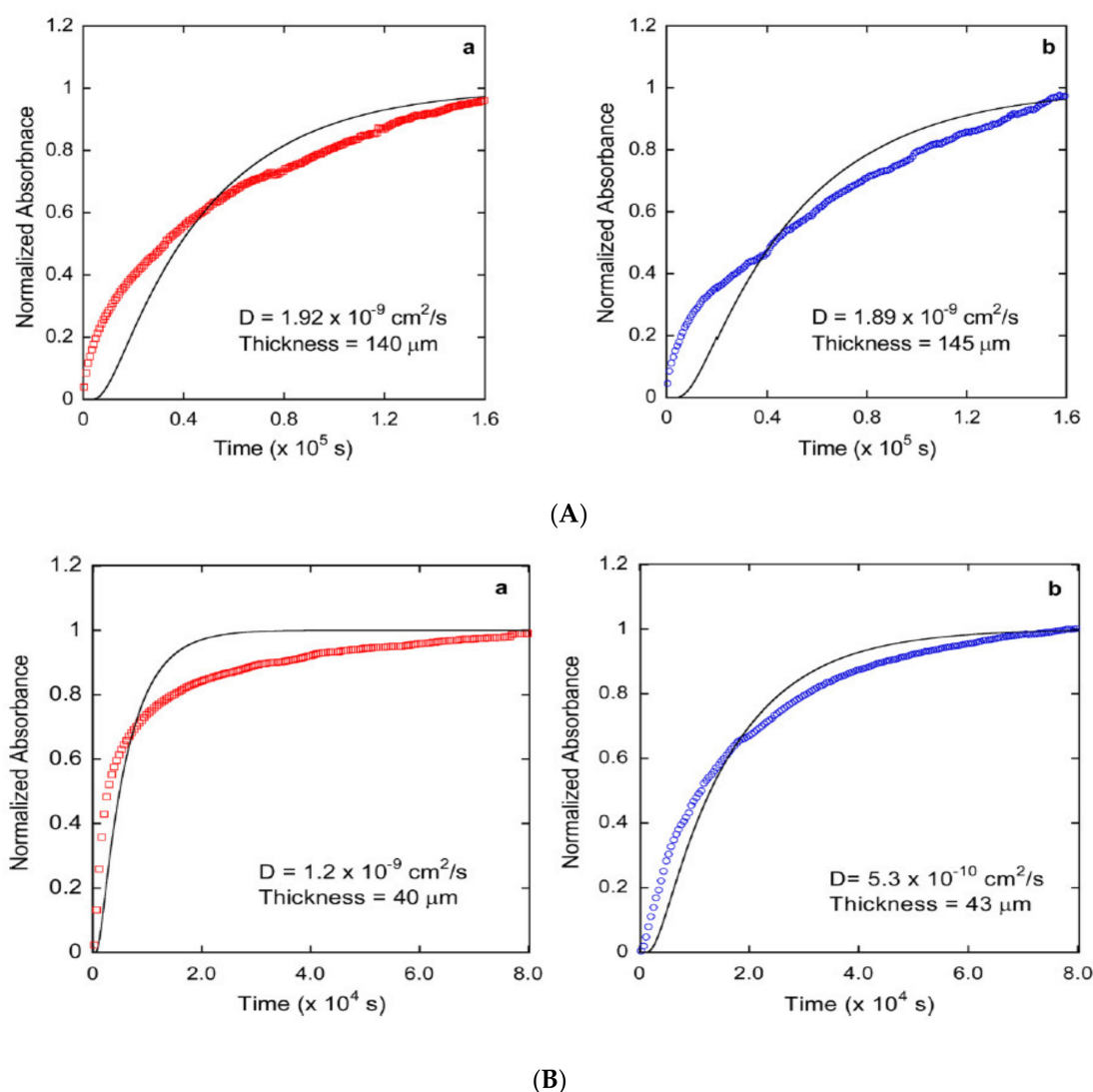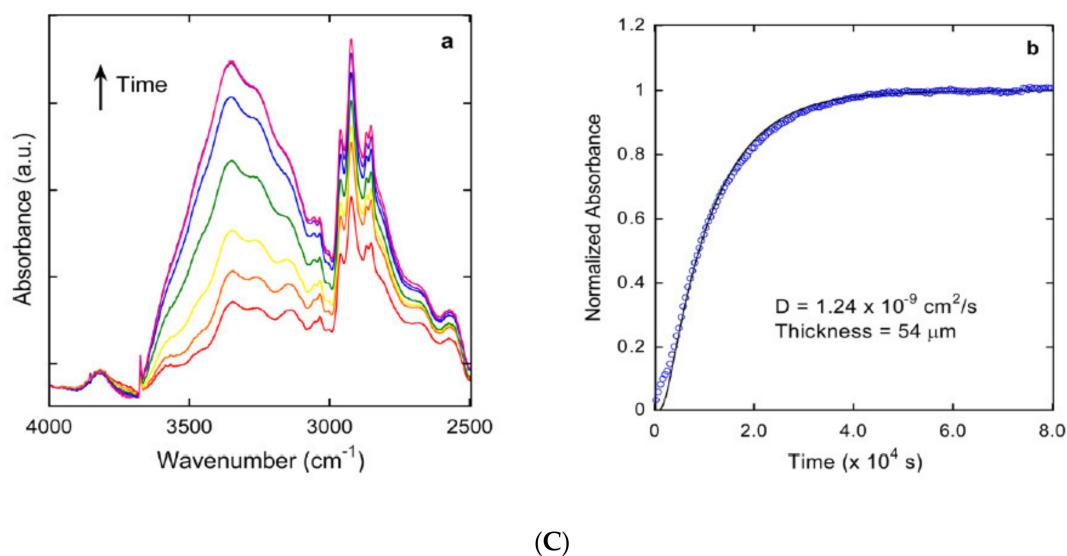

(A)

(B)

Figure 7. *Cont.*

(**C**)

Figure 7. Time-resolved infrared spectroscopy data: normalised integrated absorbance of the water O−H stretching region in polymer–poly(isobutylene)–PIB, poly(methyl methacrylate)–PMMA and a crosslinked polymer–epoxy/amine resin at room temperature for solution-cast film and free-standing film in (**A**–**C**), respectively (used with copyright permission) [41]. (**A**) Time-resolved infrared spectroscopy data: normalised integrated absorbance of the water O−H stretching region in PIB at room temperature for the (a) solution-cast film and (b) free-standing film. The solid line represents a regression to the ATR solution of the Fickian model. (**B**) Time-resolved infrared spectroscopy data: normalised integrated absorbance of the water O−H stretching region in PMMA at room temperature for (a) solution-cast film and (b) free-standing film. The solid line represents a regression to the ATR solution of the Fickian model. (**C**) Time-resolved infrared spectroscopy data: (a) infrared spectra of the water O−H stretching region, showing water diffusion in an epoxy/amine coating free-standing film, and (b) normalised integrated absorbance of the water O−H stretching region. The solid line represents a regression to the Fickian model.

3. Sorption in Glassy Polymers

3.1. Different Sorption Models

Diffusion coefficients are important, although predicting sorption isotherms of glassy polymers is also important for a variety of applications, including membrane separations, solvent extraction, volatile organic compound detection, and thin-film coating. The separation and purification of gases is a prominent implementation of sorption. Permeability values of glassy polymers may be obtained for such applications by analysing the sorption behaviour model of glassy polymers. Several distinct sorption behaviours have been observed experimentally, depending on the penetrant and polymer properties. The calculation of solubility in a glassy polymer phase relies on several computational methods, namely, the dual-mode sorption model; Guggenheim–Anderson–de Boer (GAB) model, nonequilibrium thermodynamics of glassy polymers (NET-GP) approach, molecular simulation techniques and many more.

Mixed penetrant competition for sorption sites and transport routes in glassy polymers combined with unrelaxed volume is a common characteristic of glassy polymers [42]. Permselectivity to a mixture of penetrants is strongly related to a membrane's ability to retain a size and morphology differentiating matrix, i.e., to remain essentially unplasticized under working conditions. The permeation and separation behaviours of a mixed gas are known to be very different from those of pure gases depending on the nature of the polymer, whether rubbery or glassy. Glassy polymers vary from other polymers in which the matrix is not in equilibrium, and the normal thermodynamic effects do not apply. The sorption potential of glassy polymers is higher than that of rubbery polymers [9].

Tsujita [43] interpreted the gas sorption of several glassy polymers in terms of the dual-mode sorption model. The dual-mode sorption model has been widely used to describe and study the sorption of gas molecules in glassy polymers [44]. The author's

model was based on sorption sites that obey Henry's law dissolution and Langmuir-type sorption. Henry's law dissolution site is associated with the dissolution of gases into rubbery polymers and low-molecular-weight liquids, whereas the Langmuir sorption site in a glassy polymer is associated with the holes which occur due to the non-equilibrium nature of glassy polymers. The model is formulated as [45]:

$$C = C_D + C_H = k_D p + \frac{C'_H b p}{1 + b p} \tag{8}$$

Tsujita found that holes and gas sorption in glassy polymers are functions of sub-T_g annealing, thermal quenching, and CO_2 pressure conditioning. He also found that as the sub-T_g annealing period for the copolymer-vinylidene cyanide-alt-vinyl acetate decreases, C'_H also decreases. Even, with sub-T_g annealing, k_D and constant b did not improve significantly. It was also found that thermal quenching raised the C'_H of polyamic acid, polyimide, poly(2,6-dimethyl-1,4-phenylene oxide), and polycarbonate significantly.

Ricci et al. [46] assessed extension dual-mode sorption models to predict the mixed-gas solubility and selectivity of glassy polymers. The authors evaluated the sorption of the mixture of CO_2/CH_4 in three glassy polymers: poly(trimethylsilyl propyne), the first reported polymer of intrinsic microporosity; PIM-1 and tetrazole-modified PIM-1; and TZ-PIM. The calculations revealed a qualitative picture of sorption under mixed-gas conditions, but with lower solubility due to competition with the second gas present in the mixture. The investigation also found that pure-gas data can be depicted with the least amount of uncertainty by a variety of parameter combinations, each of which yields significantly different mixed-gas predictions that, in some circumstances, only qualitatively correspond with the experimental data. Based on their findings, the authors came to the conclusion that multicomponent calculations using the dual mode sorption model produce more trustworthy results than using pure-gas data to estimate the material's solubility–selectivity.

The dual mode sorption model parameters of CO_2 in glassy polymers were predicted by Saberi et al. [47] using a group contribution technique. The group contribution approach is a method for determining the principles that regulate the link between polymer transport and thermophysical properties based on the structure of the polymer [48]. A total of 37 structural units were examined using 82 different polymers, and dual mode sorption values for CO_2 sorption were calculated for each group by the authors. In addition, the experimental results for CO_2 sorption in six distinct glassy polymers, which were not included in the group contribution calculation, were taken into account. The dual-mode sorption parameters were assumed as follows:

$$k_D = \sum_{i=1}^{C} \varphi_i k_{Di} \tag{9}$$

$$C'_H = \sum_{i=1}^{C} \varphi_i C'_{Hi} \tag{10}$$

$$b = \sum_{i=1}^{C} \varphi_i b_i \tag{11}$$

where

$$\varphi_i = \frac{Van\ der\ Waals\ volume\ of\ group\ i}{Van\ der\ Waals\ volume\ of\ polymer} \tag{12}$$

The optimisation toolbox in MATLAB software was used to solve the set of these equations. The reliability of the model was checked using two statistical indicators: root mean square error and the correlation coefficient, R-squared. The authors concluded through this process that group contribution approach is a valuable tool to anticipate CO_2 dual-mode sorption parameters in various glassy polymers.

To explain sigmoidal isotherms, primarily using water vapour sorption data, Feng [49] employed the Guggenheim–Anderson–de Boer (GAB) model. The GAB model is a legitimate extension of the Brunauer–Emmett–Teller (BET) method for the multilayer adsorption

of small molecules in a solid adsorbent [50]. Based on the multilayer sorption theory of GAB models, the author developed a new dual-mode sorption model for vapour sorption in glassy polymers. The famous GAB equation is stated as follows:

$$c = \frac{C_p A k a}{(1 - ka)[1 - ka + Aka]} \tag{13}$$

In this, k and A can be calculated as follows:

$$k = k_0 \exp\left(\frac{H_L - H_n}{RT}\right) \tag{14}$$

$$A = A_0 \exp\left(\frac{H_m - H_n}{RT}\right) \tag{15}$$

The proposed dual-mode sorption model is based on four assumptions:

I   In a glassy polymer material, there are two types of sorption sites: one is in the matrix region of the polymer, and the other is in the micro-voids;

II   The partition functions of all the molecules in the polymer matrix region are the same;

III   GAB sorption occurs in the polymer micro-void site;

IV   In the micro-void region, the molecules in layers other than the first have the same partition function as those in the matrix region. The new dual-mode sorption equation was created based on these assumptions:

$$c = c_1 + c_2 \tag{16}$$

$$c = \overline{C_p} \frac{k'a}{1 - k'_a} + \overline{C_p} \frac{(A' - 1)k'a}{1 + (A' - 1)k'a} \tag{17}$$

The new dual-mode sorption model for vapor sorption in glassy polymers assumes that two species of the sorbed molecules contribute to the penetrant concentration in glassy polymers, one of which occurs in the matrix region and follows $c_1 = \overline{C_p} \frac{k'a}{1-k'_a}$, which is a downward curve similar to that in rubbery polymers; the other happens in the micro-voids and follows $c_2 = \overline{C_p} \frac{k'a}{1-k'_a}$, which is an upward curve.

Vopicka et al. [51] also studied the GAB model feasibility for modelling gas sorption isotherms and their temperature dependences. In contrast to the assumptions of the standard dual-mode sorption model, the GAB model assumes that molecules adsorb in multilayers on the inner surfaces of polymers. For CO_2 sorption in cellulose acetate, polyethylene terephthalate, and PIM-1, the authors discovered that the isosteric heat of adsorption is completely reliant on relative surface coverage and showed maxima at values of around 0.8–1.2. Instead of a combination of single-layer adsorption and equilibrium dissolution, this leads to the development of adsorption multilayers. The GAB approach incorporates both pressure and temperature dependences and fits the literature data efficiently.

Carla et al. [52] used the NET-GP method, developed after investigating non-Fickian diffusion in glassy polymers [53], to create a 1D transport model to explain the sorption and dilation kinetics of polymeric films in supercritical CO_2. The model calculations were compared with data on mass sorption kinetics for CO_2 in supported glassy poly(methyl methacrylate) (PMMA) films, measured in a high-pressure quartz crystal microbalance (QCM). Doghieri and Sarti [54] introduced the NET-GP approach, which is a semi-empirical approach for extending any arbitrary equation of state model for the equilibrium properties of glassy polymers to nonequilibrium states below T_g. The model was based on the assumption that an isotropic glassy mixture can be interpreted by using the partial polymer density as the order parameter to classify the nonequilibrium structure caused by the matrix prehistory. The order parameter had been treated as an internal state variable, and the associated thermodynamic relationships have been used systematically way.

The authors developed a sorption–diffusion–relaxation model to evaluate the solvent chemical potential under nonequilibrium conditions by combining the NET-GP model with a rheological constitutive equation.

$$\mu_s^{NE} = \mu_s^{NE}\left(T \omega_s \dot{\rho}_p\right) \qquad (18)$$

Through the application of Fick's law for the diffusive flux of the penetrant species in the model, the authors represented the two-stage sorption behaviour in thin glassy polymer films.

$$j_s = -\rho_s \; D_s \; \nabla(\mu_s/RT) \qquad (19)$$

To analyse water sorption thermodynamics in polyimides, Scherillo et al. [53] employed the NET-GP–non-random hydrogen bonding (NET-GP–NRHB) model. Panayiotou et al. [55] presented the NRHB theory, which comprises a compressible lattice model accounting for cross- and self-hydrogen bonding interactions between polymer and water molecules, based on an equation of state. The analyses were performed by in situ infrared spectroscopy. In the case of the NET-GP−NRHB model, in addition to polymer density ρ_2, two new sets of order parameters N_{ij} and N_{rs}^{NR} are incorporated as internal state variables (underlying represent set of variables). The generic component of the set N_{ij} represents hydrogen bonding between H^+ donor groups of type i and H^+ acceptor groups of type j, whereas the generic component of the set N_{rs}^{NR} represents the effective number of non-random contacts in the compressible lattice between kind r and kind s polymers. The authors indicated that the data give acceptable accuracy with values derived using FTIR spectroscopy analysis for self-hydrogen bonding and with values derived using a 1:2 stoichiometry in the case of cross-hydrogen bonding, as shown in Figure 8.

Minelli et al. [56] examined three gas–gas–polymer systems—CH_4/CO_2 in poly(2,6-dimethyl-1,4-phenylene oxide), C_2H_4/CO_2, and N_2O/CO_2 in poly(methyl methacrylate)—which demonstrated considerable deviations from the ideal behaviour. The author employed the non-equilibrium lattice fluid (NELF) model, which is based on the NET-GP methodology and uses the lattice fluid characterisation of pure chemicals and mixtures [57].

The parameters of the gas–gas interaction were set to zero. Based on the partial pressure of each component in the gaseous mixture and the pure gas swelling coefficient in the polymer, the swelling induced by the gas mixture in the glassy polymer was presumed to follow an additive rule. The mixed gas solubility differed greatly from the pure gas value; in particular, the addition of a second gas lowered the equilibrium content of a gas sorbed in a polymer in all of the scenarios studied. The authors calculated pure component and binary parameters using pure gas sorption data to determine the highest discrepancy between experimental data and model predictions, which was 10%. As a result, the model appeared to be a credible method for estimating mixed gas solubility in glassy polymers.

Galizia et al. [58] compared alkane and alcohol vapour sorption and swelling in poly(trimethyl silyl norbornene) to the NELF model predictions. The following equation was used to calculate NELF parameters from infinite dilution solubility coefficients, S_0, of a wide range of n-alkane penetrants:

$$\ln(s_0) = \ln\left(\frac{T_{STP}}{p_{STP}T}\right) + r_1^0\left[\left[1 + \left(\frac{v_1^*}{v_2^*} - 1\right)\frac{\rho_2^*}{\rho_2^0}\right]\ln\left(1 - \frac{\rho_2^0}{\rho_2^*}\right) + \left(\frac{v_1^*}{v_2^*} - 1\right) + \frac{\rho_2^0}{\rho_2^*}\frac{T_1^*}{T}\frac{2}{p_1^*}(1 - k_{12})\sqrt{p_1^* p_2^*}\right] \qquad (20)$$
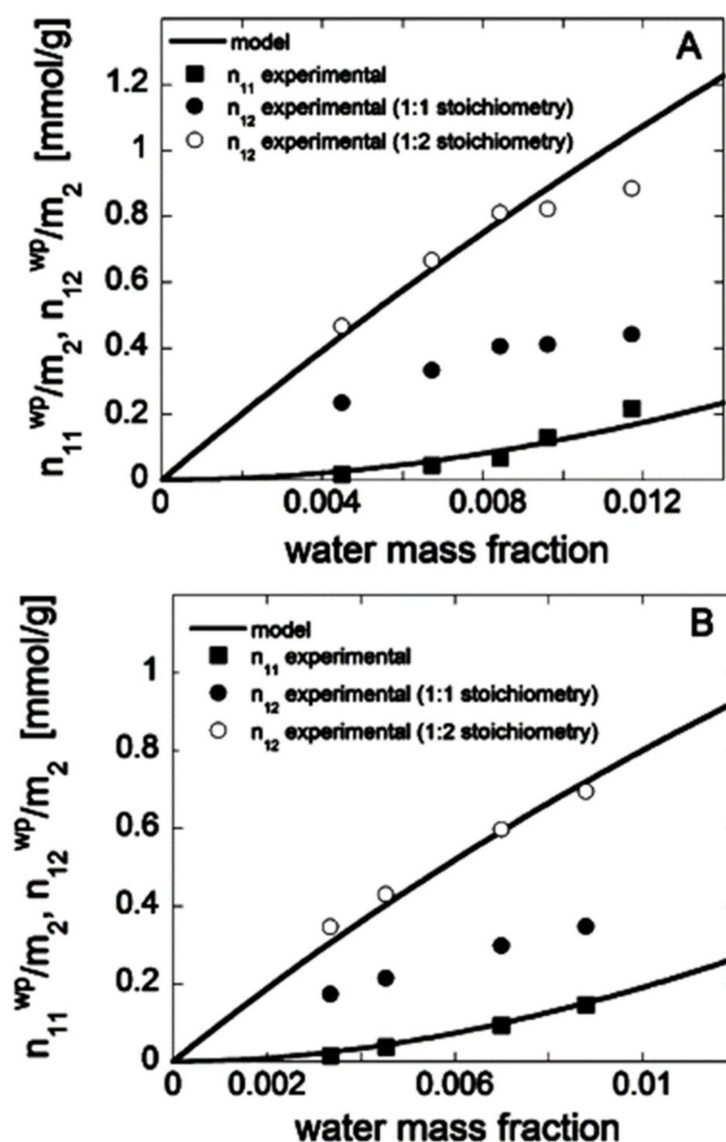
Figure 8. (**A**,**B**) Comparison of predictions of the NET-GP−NRHB model with experimental results for (**A**) 6FDA-ODA and (**B**) 6FDA-6FpDA (used with copyright permission) [53].

The solubility isotherms of alcohols with a distinctive sigmoidal behaviour were observed to be in accordance with the NELF model prediction. In different polymer system, the model was also successfully employed to characterise the relationship of solubility on the size of the alkane. As shown in Figure 9, the model appropriately predicted that the activity-based solubility coefficients in poly(trimethyl silyl propyne) increase with critical temperature, drop with critical temperature in Teflon-AF2400, and hold almost constant in poly(trimethyl silyl norbornene). The polymers fractional free volume, cohesive energy density, and their energetic interaction with the penetrant, were found to be the three key determinants impacting the level of solubility reliance on alkane size.

Vegt et al. [59] employed iterative Widom schemes to determine the sorption isotherms of CO_2 in glassy polyethylene, utilising molecular dynamics simulations. They discovered that the sorption thermodynamics are driven by a hole-filling process in the glassy polyethylene. This mechanism, which was predicated on the presence of energetically favourable sorption sites below T_g, manifested itself as a decrease in the number of low-energy sites as concentration increased. The configurational molar entropy of the solutes was observed to decrease as a result of this action. A finite positive CO_2 partial molar volume in the glass, in addition to hole-filling, was calculated by the authors, showing

at least some degree of relaxation when solutes dissolved. The findings were consistent with Kirchheim's model predictions [60] in which the hole-filling concept was combined with the assumption that a matrix becomes elastically distorted when a solute is dissolved. The self-intermediate scattering function of the polymer atoms was used to investigate dynamical changes at T_g. This function was also discovered to reveal the difference in dynamics between the glassy and rubbery states.
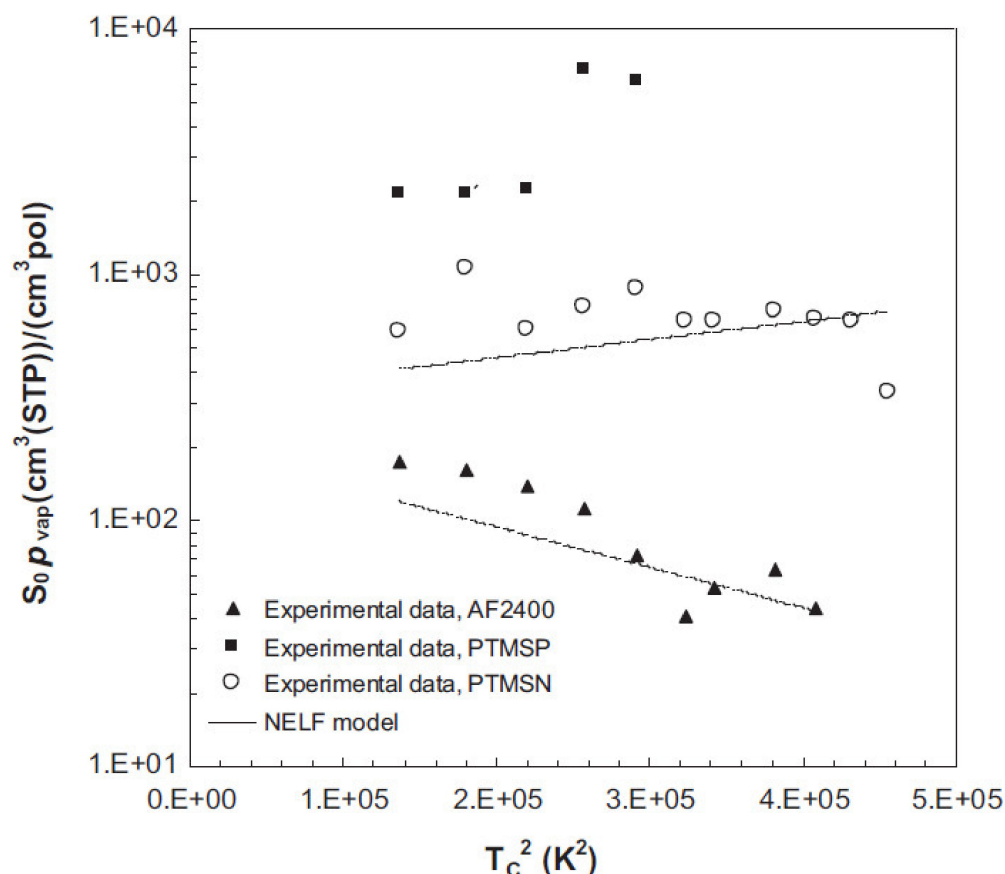
Figure 9. Activity-based solubility coefficients of n-alkanes at infinite dilution in poly(trimethyl silyl propyne)—PTMSN, poly(trimethyl silyl propyne)—PTMSP and Teflon AF2400 at 25–35 °C and exponential interpolations of NELF model predictions on the same system with k12 = 0 for PTMSN, k12 = 0.04 and k12 = 0.87 for Teflon AF2400 (used with copyright permission) [58].

Spyriouni et al. [61] also applied iterative Widom schemes to determine CO_2 sorption isotherms and induced polymer swelling in atactic polystyrene at temperatures ranging from 308 to 405 K. For the estimation of penetrant fugacity, the authors combined this methodology with the direct particle deletion approach [62]. The results were consistent with available experimental data; however, significant variations were shown at low temperatures and high pressures. This was due to the extended relaxation durations of the polymer matrix. The linearity of the sorption curves incremented at elevated temperatures, when the polymer was in the melted state. For the free volume calculations, the solute molecules were removed from the matrix. The free volume of the polymer matrix in the CO_2–polystyrene systems exhibited elevated levels at higher temperatures, attributed to polymer swelling, as illustrated in Figure 10.
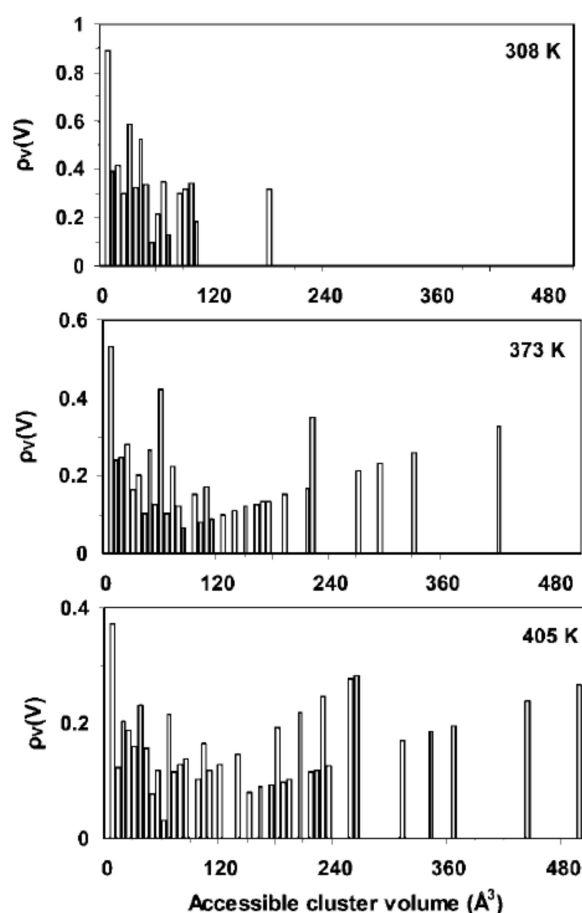
Figure 10. For a solute radius of 2.1 Å, volume-weighted distribution of free volume for a CO_2–polystyrene system with a concentration of 35 cm^3 (STP) CO_2/cm^3 pol at 308, 373, and 405 K (used with copyright permission) [61].

Neyertz and Brown [63] predicted the gas sorption isotherms in a glassy polymer membrane with a single/mixed-gas reservoir using three molecular simulation approaches, namely, Grand Canonical Monte Carlo (GCMC), iterative test particle insertion–molecular dynamics (TPI/MD), or an iterative GCMC/MD method. The research was carried out on a large-scale 6FDA-6FpDA polyimide bulk model with ~50,000 atoms, subjected to a wide variety of pressures. The gases used were $N_2 < CH_4 < CO_2$, listed here in increasing order of solubility and plasticizing effect.

The chemical potential, volume, and temperature are all kept constant in GCMC [64], but the number of particles fluctuates about an equilibrium value during the simulation. The polymer system is assumed to be in contact with a penetrant reservoir at a given temperature and chemical potential, through which it transfers energy and particles during simulations [65]. GCMC was unable to quantify penetrant-induced changes in the polymer matrix, whereas the research group observed that the pressure-iterating p-TPI-MD and GCMC-MD models were able to accurately predict ideal sorption selectivities in the glassy matrix. It was demonstrated that both of these approaches are iterative in the sense that they need the procedure to be repeated until convergence is achieved. According to the findings, the iterative number TPI-MD technique was discovered to be exclusively applicable to binary mixtures. The iterative GCMC-MD technique was more easily adaptable to mixed-gas inputs and could be used with binary and ternary combinations. It was also concluded that the penetrant locations are randomised in GCMC-MD, making it considerably easier to adapt to the situation of multi-component gases.

3.2. Hysteresis Effect of Sorption

Hysteresis, which is commonly noticed while switching from the sorption to the desorption phase, is one of the distinctive characteristics of sorption behaviour in glassy polymers. Gas sorption hysteresis, in which the mass sorbed is not a precise function of the gas-specific activity has been reported [66]. Changes in the free volume in a glassy state of the polymer have been related to the occurrence of sorption hysteresis [67]. The swelling and glass transition of the polymer system are associated with hysteresis. It was discovered that the different sorption and volumetric behaviours of glassy polymers are produced by concentration dependence of the specific volume and the polymer's Gibbs free energy. The structural rearrangements in the polymer matrix when a penetrant is introduced are reflected by the dependence on concentration.

Fleming and Koros [68] observed hysteresis effects in the volume and sorption level for CO_2 in polycarbonate. This implied that the presence of CO_2 during depressurisation slowed the polymer's relaxation to its previous thermodynamic state. These findings were in line with previous research in vapor/polymer systems. The authors claimed that increases in the Langmuir sorption capacity seemed to be directly related to the unrelaxed volume present in a glassy sample following complete CO_2 removal. The increase in sorption capacity observed for polymers with a similar history matches extremely well with the unrelaxed volume present in the sample after the full removal of CO_2.

Sorption of CO_2 and CH_4 for polysulfone and a polyimide was measured by Holck [69]. Concurrently, the gas-induced swelling effect was measured with a dilatometer based on a capacitive distance sensor recorder. The dilation and contraction behaviours shown in molecular dynamics simulations of atomistic packing models support the experimental evidence of the elastic nature of gas-assisted dilation. The partial molar volume of penetrants in a single polymer is concentration-dependent, according to the experiment.

Björklund and Kocherbitov [70] demonstrated hysteresis effects linked to the hydration history rather than the temperature history by presenting the water sorption–desorption behaviour of thin mucin films. The authors utilised the humidity scanning quartz crystal microbalance with dissipation monitoring (QCM-D) technique to acquire water sorption–desorption isotherms of mucin films under controlled circumstances where water diffusion is not a limiting factor in the vapour phase or the glassy mucin film. Regardless, water diffusion was not the limiting factor, the sorption–desorption branches exhibited hysteresis effects comparable to those seen in bulk materials. The hydration-induced glass transition was demonstrated to be in perfect accord with the start of the sorption–desorption hysteresis, as determined by monitoring the film's rheological behaviour.

4. Applications of Glassy Polymers

Glassy polymers are considered as the most important classes of polymers that include the matrix resin in contact lens, aerospace composites, automotive head/tail-lights, and many more other products. Thin films formed from glassy polymers are used in various technological applications such as liquid and gas separation, solar cells, optical materials, fuel cells, lithography [71]. Below, some important applications of glassy polymers which have been explored by the various research groups are listed.

4.1. Applications in Drug Delivery Systems

Hydrogels are hydrophilic polymeric networks which have the ability to absorb vast volumes of water and are extremely appealing bio-compatible drug delivery devices. They significantly deliver a better efficiency of drug delivery and have a wide range of clinical applications [72]. Hydrogel polymers are unique because they have a glassy nature in the dry state and are capable of the immobilisation of any non-uniform drug distribution introduced before the dehydration step. In the presence of water, they can absorb a substantial amount of water to turn into an elastic gel and, simultaneously, release the drug dissolved in them by diffusion through the swollen region [73]. Lee et al. [74] found out novel approach to zero-order drug delivery from glassy hydrogel beads through an

immobilised sigmoidal drug distribution. The combination of controlled freeze-drying and the extraction process was paramount in the in situ immobilisation of such non-uniform concentration distributions. They found that when the extraction process was carried out on drug-loaded beads in fully swollen state instead of dry glassy state, or when the drying of the film was performed at a higher temperature instead of a freeze-drying state, no constant release region would be observed in the cumulative drug release profiles. Seemingly, a drug concentration distribution of parabolic type, Fickian diffusion characteristics in the rubbery state, did not lead to a zero-order release.

Said et al. [75] synthesised a pH-sensitive interpolymer polyelectrolyte complex to investigate its use as a carrier for colon-specific medication delivery. The complex was synthesised by gamma-radiation-induced copolymerisation of acrylic acid and dimethyl aminoethyl methacrylate (DMAEMA). At pH values ranging from 3 to 4, the pH-dependent swelling revealed distinct phase transitions depending on the copolymer composition, as well as the creation of interpolymer polyelectrolyte complexes. The Ketoprofen-loaded complex was allowed to swell in pH 1 (similar to stomach medium) and pH 7 buffer solutions (pH is similar to intestine medium), as illustrated in Figure 11. The author discovered that no appreciable drug release occurred at pH 1, but that it occurred as soon as the copolymer was moved to a pH 7 buffer solution. The findings revealed that drug release was not only pH-dependent, but also that the copolymer composition had an impact on the release rate and total amount of drug released. The release rate and total amount of medication released increased as the acrylic acid level in the copolymer increased.
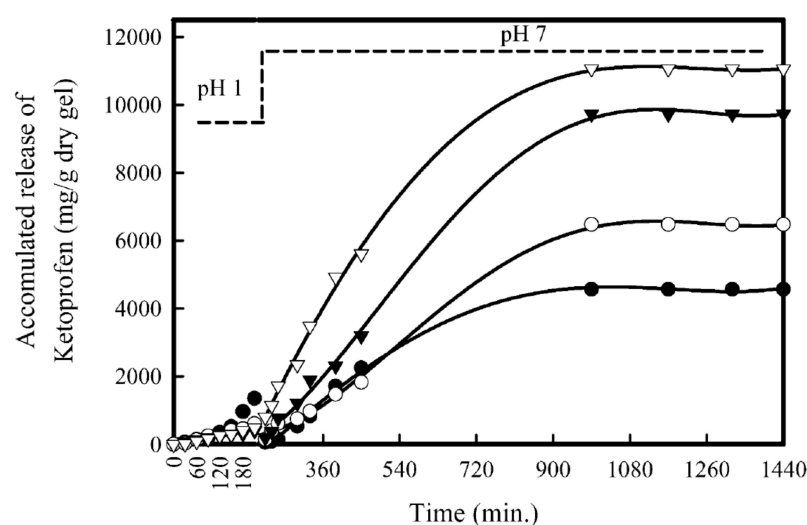
Figure 11. Release profile of ketoprofen from (acrylic acid/DMAEMA) copolymers of different acrylic acid contents in buffer solution of pH 1 for 3.5 h followed by buffer solutions of pH 7 up to 24 h: (●) 75%, (○) 80%, (▼) 90% and (▽) 100% acrylic acid content (used with copyright permission) [75].

The gamma-radiation-induced copolymerisation was also assessed by Taleb et al. [76] and Mazied et al. [77] in their research for applications of the controlled release of chlorte-tracycline HCl and flutamide, respectively. Mazied et al. synthesised hydrogels based on DMAEMA and various ethylene glycol dimethacrylate ratios to demonstrate diffusion-controlled flutamide administration. The pH of the solution and the DMAEMA content of the hydrogel were the primary considerations impacting the drug release behaviour of the hydrogel, according to in vitro drug release studies in various buffer solutions. Based on 2-hydroxyethylmethacrylate and methacrylic, Taleb et al. produced multifunctional poly-meric material hydrogels. The hydrogels loaded with chlortetracycline HCl were placed in buffer solutions of pH 1 and 7.5 to release chlortetracycline HCl. The diffusion coefficients rose as the methacrylic content in the hydrogel increased, and the release behaviour was strongly pH-dependent (low release at pH 1.0 and peak release at pH 7–8). In both the

articles, it was found that the inclusion of amino groups along the macromolecular chains, which ionised at lower pH while imparting hydrophobicity to the gels at higher pH, was completely responsible for the pH-dependent releasing mechanism. It was concluded that the hydrogels developed by the authors can be used as promising carriers for drug delivery systems.

Mullarney et al. [78] studied the release of Pheniramine maleate drug using hydrophobically modified hydrogels prepared by the free-radical polymerisation of N,N-dimethylacrylamide and 2-(N-ethylperfluorooctanesulfonamido) ethyl acrylate-FOSA copolymers. The authors discovered that when the amount of FOSA in the hydrogel increased, the equilibrium media content reduced and the drug release rate slowed. It was found that over the pH range of 4–8, drug diffusion was less sensitive to pH; however, raising the media pH marginally impeded permeability by reducing the hydrogel's swell potential. This suggested that the mass transport mechanism for drug diffusion was investigated to demonstrate if the diffusion rate was predominantly controlled by Fickian-type diffusion rather than polymer swelling.

Rudzinski et al. [79] used a solution and bulk polymerisation method to create three acrylic-based methyl methacrylate copolymers with varied methacrylic acid ratios. One of the polymers was created by adding 2-hydroxy ethyl methacrylate in order to boost its hydrophilicity. Due to the presence of carboxylic acid groups, the partially crosslinked hydrogels had varied hydrophilicity; therefore, they were pH-dependent. As the number of –COOH groups increased, so did the swelling. To test the controlled release functionalities of these hydrogels, Cypermethrin, a commonly used pesticide, and cupric sulfate, a micronutrient, were loaded into them. In addition to pesticide or micronutrient transport, their release was dependent on macromolecular chain relaxation. Farmers producing in dry terrains may benefit from the release of active substances via hydrogels, according to these findings.

Brazel and Peppas [80] studied the effect of various structural parameters of the polymers, swelling rates, water diffusion coefficients and the diffusional Deborah number on the drug release mechanism in glassy polymers. In order to transport water, two crosslinked polymer systems were used: poly(2-hydroxyethyl methacrylate-co-methyl methacrylate) and poly(vinyl alcohol). Eight types of drugs were tested to study the drug-release mechanism. Based on the size of the diffusing drug molecule and the size exclusion properties of the polymer carrier, the drug release mechanism was Fickian, anomalous, or Case II diffusion. The research showed that swelling rates were closely proportional to the mesh sizes of polymer networks. The authors also found that in crosslinked poly(vinyl alcohol) samples, initial crosslinking ratios exhibited a significant effect on water uptake. As the molecular weight of the solute increased, the rate of release decreased. It was concluded that for each polymer studied, a molecular weight cut-off was determined, beyond which drug release was severely hampered by the hydrogel mesh size.

4.2. Applications in Coatings

4.2.1. Corrosion Prevention

For corrosion protection, there is a reliance on the properties of glassy polymers such as mechanical, transport, and physical properties when coated on a metal substrate. The properties are affected by the presence of free volume in the polymer which, in turn, has an effect on the coating performance. Free volume permits the diffusion of small molecules such water, oxygen and ions. It also permits local segmental movement which affects mechanical properties such as adhesion, and yield [81].

Vergara et al. [82] studied aliphatic amido amine crosslinkers used in epoxy coatings to augment water barrier properties for prevention from corrosion. They found a critical concentration where if more methylene groups were added to the pendant alkyl chain, it did not improve the water barrier properties because the solubility decreased to a lesser range than diffusivity increased beyond for the pendant alkyl chain containing more than four carbon atoms. The thermo-mechanical properties of practiced amido-amine polymers

were similar to the commercial amido-amines/epoxy and had reduced T_g and higher modulus values than Diglycidyl ether of bisphenol A/Diethylenetriamine. The above-mentioned properties make the resulting Diglycidyl ether of bisphenol A-amido amine crosslinkers polymers more applicable for corrosion prevention coatings. Additionally, the water transport was minimised by only short alkyl modifiers containing four carbons.

Merachtsaki et al. [83] evaluated the corrosion behaviour of steel covered with epoxy-(organo) clay nanocomposite films. According to the study, both pure epoxy and epoxy nanocomposite coatings provided significant corrosion protection to steel. The nanocomposite coatings protective qualities, including mechanical, thermomechanical, and barrier characteristics, were found to be superior to those of the pristine epoxy polymer. The weight loss findings shown in Figure 12, as well as the optical and microscope inspection of the specimens following exposure to the corrosive environment, indicated this. The electrochemical impedance experiments revealed that the coatings employed enhanced total resistance and that nanocomposites had higher total resistance values than the pure glassy epoxy polymer, implying superior protective characteristics.
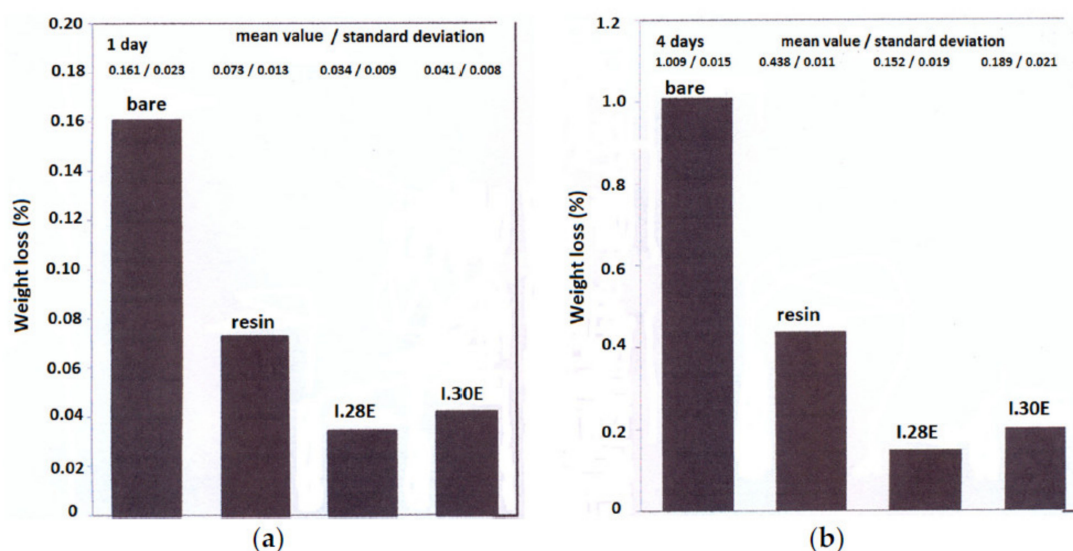

Figure 12. Weight loss results from salt spray experiments for bare steel and steel coated with pristine epoxy resin, and nanocomposites with I.28 and I.30 organo-clays, after 1 day (**a**) and 4 days (**b**) of exposure in a corrosive environment of 100% saturated moisture + 5 wt. % NaCl solution (used with copyright permission) [83].

Kostina et al. [84] investigated the production of a glassy metaphosphate composition from simple and easily accessible materials for comprehensive corrosion and salt deposition protection of the elements of water-heating systems. According to the findings, glassy metaphosphate composition's anticorrosion properties were due to the formation of a thin continuous phosphate film on the surface of the water-heating apparatus' elements. The thickness of the film remained constant during operation because its top layers, which could be removed as new portions of water arrive, were renewed. It was also discovered that if the composition was not fed into the water, the coating stayed protective for at least one month. Glassy metaphosphate composition protected metallic surfaces from corrosion even at low concentrations when added to water. Glassy metaphosphate composition reduced the volume of scale on any surface, even non-metallic surfaces, to levels 70 times lower than untreated water.

4.2.2. Gas-Separation Membranes

Sharma et al. [85] accomplished hydrogen separation using an aligned carbon nanotube–polymer nanocomposite. By dispersing (0.1%) weight fractions of single-walled carbon nanotubes and multi-walled carbon nanotubes in a polycarbonate matrix independently, carbon

nanotube–polymer nanocomposites were formed. In comparison to randomly distributed CNT/polymer nanocomposites, gas permeability had been reported in the research to be higher in aligned CNT/polymer nanocomposites because the former provided easy pathways or porosity for hydrogen penetration. It was also shown in the study that aligning carbon nanotubes in polymers can improve mass transport and electrical conduction. Figure 13a demonstrates how aligned single-walled carbon nanotubes in a polycarbonate matrix offer a simple route for hydrogen to penetrate quickly. Figure 13b indicates that permeability rises with aligned multi-walled carbon nanotubes, and Figure 13c illustrates that gas permeation is proportional to the thickness of the nanocomposites.
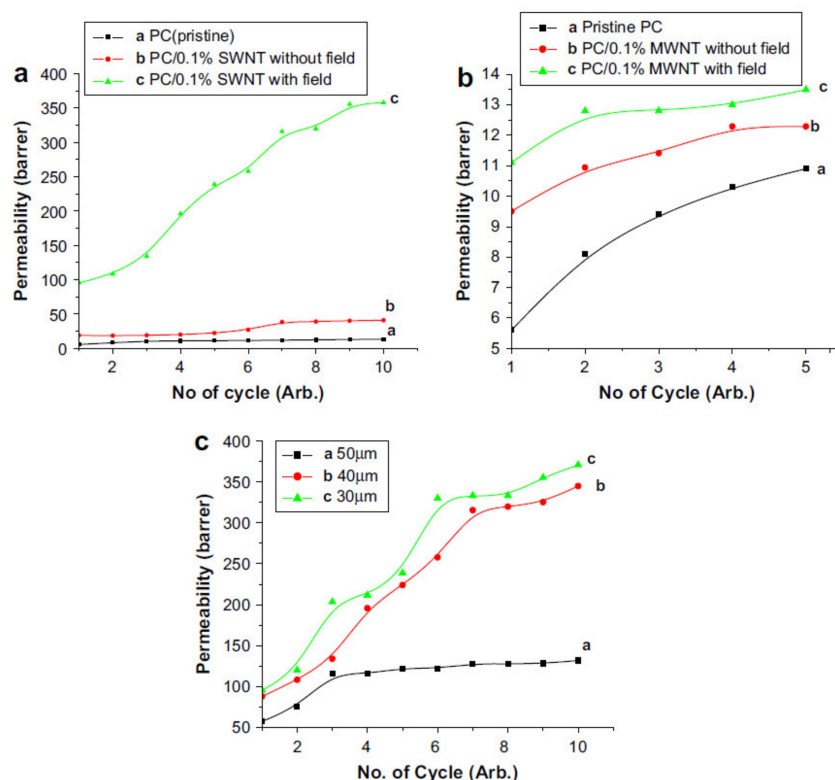
Figure 13. Permeation of hydrogen gas through: (**a**) pristine/0.1% single-walled carbon nanotubes (SWNT) composite membrane; (**b**) pristine/0.1% multi-walled carbon nanotubes (MWNT) composite membrane; (**c**) the dependence of gas permeation on thickness (used with copyright permission) [85].

Park et al. [86] evaluated how 3D disordered mesoporous silica–DMS affected the transport of two different glassy polymer matrices, polysulfone and 6FDA–DAM:DABA (3:2). 6FDA–(4,4′-hexafluoropropylidene) diphthalic-anhydride, DAM-2,4,6-trimethyl-1,3-diaminobenzene, DABA-3,5-diaminobenzoic acid.

The mixed matrix membrane permeabilities for gases such as N_2, CO_2, CH_4 and NF_3 were assessed. The investigations showed that both 6FDA–DAM:DABA (3:2) and polysulfone-based membranes with a nominal DMS weight fraction of 0.2 significantly enhanced all single gas permeabilities due to enhanced diffusivity, which seemed to be the outcome of DMS particles' 3D interconnected pore frameworks. Due to the difference in the structure, and the degree of rigidification of polymer chains surrounding DMS particles, the favourable effect of DMS on permeability enhancement at relatively low DMS volume fraction was stronger for 6FDA–DAM:DABA (3:2) compared to polysulfone. Due to its potential to form H-bonding or polar–polar interactions with DMS particles, NF_3 displayed unique transport behaviours that were not observed in any of the other gases studied. According to the findings, DMS-containing mixed matrix membranes, particularly the 6FDA–DAM:DABA (3:2)/DMS (20 wt. %) sample, had good separation performance for various gases.

Kramer et al. [87], in their study, enhanced polymeric asymmetric membranes to improve gas-separation selectivity. The researchers used ozone to oxidise an asymmetric membrane made of a glassy polymer to improve its selectivity for a pair of gases when compared to the glassy polymer's intrinsic selectivity and the chemically modified glassy polymer's selectivity for the same pair of gases. The density, free volume, and close packing of the reacted polymers all had an influence on membrane selectivity, according to the authors. The degree of ordering of the polymer chains initially present in the membrane, the reactivity of the polymer with respect to ozone, and the level of reaction the polymer underwent all contributed to the selectivity. The membranes could separate a variety of gas combinations, including He/N_2, H_2/N_2, H_2/CH_4, N_2/O_2, H_2/CO_2, He/CO_2, He/O_2, H_2O/Air, H_2O/N_2, H_2O/CH_4, H_2O/CO_2, and He/CH_4.

On a porous support membrane constructed from a glassy polymer including polyethersulfone, polysulfone, polyimide, a composite of these polymers, and a blend of cellulose acetate and cellulose triacetate, a novel high-flux, crosslinked, fumed silica-reinforced polyorganosiloxane thin-film composite membrane was designed by Liu et al. [88]. The authors demonstrated that when the operation duration was increased, the permeance and selectivity of the membrane described in this invention improved. This was mostly due to the increased membrane plasticization of condensable olefins or a drop in operating temperature. The membrane also exhibited comparable selectivities but much higher permeances of CH_4 for CH/N separation, and considerably higher permeances of olefins and paraffins for olefin and LPG recovery.

Choi et al. [89] developed a gas-separation membrane with a porous support layer, an aromatic poly amide layer on the porous support layer, and a coating with a glassy polymer formed on the aromatic polyamide layer for the selective separation of hydrogen and helium from gas mixtures containing carbon dioxide. The glass transition temperature of glassy polymer was more than 50 °C. Contacting a solution containing the glassy polymer with an aromatic polyamide layer of a composite membrane and drying the solution to create a coating of the glassy polymer on the aromatic polyamide layer could create the gas-separation membrane. Contacting a gas feed stream containing carbon dioxide with the gas-separation membrane to produce a permeate stream with a concentration of helium or hydrogen that exceeded the concentration of helium or hydrogen in the gas feed stream was one method of separating hydrogen or helium from a gas stream containing CO_2.

To examine the dehydration of organic vapour mixtures by glassy polymers, Salem and Ghoreyshi [90] developed a model based on the Maxwell–Stefan formulation methodology. The equilibrium and kinetic coupling of fluxes between two permeating components in the model was taken into account in the theoretical investigation of the probable transport mechanism. The dehydration of an ethanol–water vapour mixture was chosen as the system to evaluate the model. The model results revealed that the presence of the other component had no kinetic effect on either component's mobility, but the thermodynamic interaction had a considerable impact on both components' movement. The model predicted a separation factor that was quite close to the experimental value. The results further showed that the glassy PVC membrane is selective for water vapour and may be utilised to dehydrate a water–organic mixture acceptably.

Gomes at al. [91] synthesised nanocomposite membranes based on poly(1-trimethylsilyl-1-propyne)-PTMSP and silica. The membrane was prepared by sol–gel copolymerising tetraethoxysilane with various organo-alkoxysilanes in PTMSP–tetrahydrofuran solutions. They discovered that the gas permeability characteristics of these membranes are influenced by the degree of silica conversion, the kind and concentration of organo-alkoxysilane used, and the size of the silica particle produced. When contrasted to PTMSP nanocomposite membranes produced with dispersed fillers, the marginal increase in butane permeability and butane/methane selectivity may be due to the relatively low content of silica embedded into the PTMSP membrane by the sol–gel method and the role of residual silane left in the membrane. Figure 14 shows the permeation characteristics of a mixed gas in a PTMSP nanocomposite membrane produced by adding 30 wt. % filler.
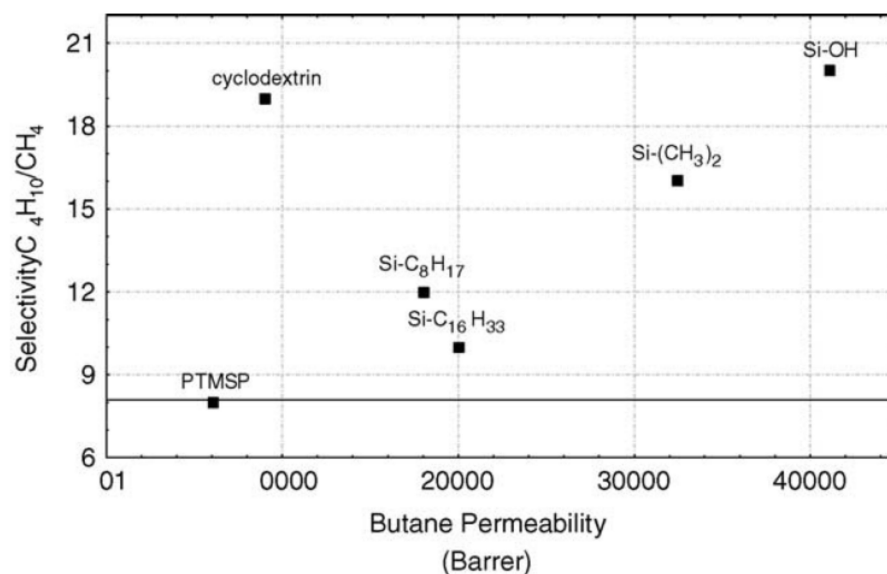
Figure 14. Permeation properties for mixture gas in PTMSP nanocomposite membrane prepared by adding 30 wt. % filler (based on polymer content) at 30 °C with feed pressure of 1.4 bar and permeate pressure of 1 bar (used with copyright permission) [91].

*4.3. Applications as Polymer Matrix in Composites*

Glassy polymers make up a large percentage of advanced composite matrices. The mechanical characteristics of polymers are becoming particularly significant because they are employed in structural design. Furthermore, the characteristics of particulate composites are extensively regulated by particle size, loading fractions, particle type, and particulate–matrix adhesion [92].

Over a variety of strain rates and temperatures, Jordan et al. [93] investigated the compression of extruded PMMA rods with aligned polymer chains and Al–Ni–PMMA composites. At the highest strain rates and lowest temperatures, the PMMA showed the predicted strain rate and temperature relationships. Brittle failure was observed in the highest strain rate and lowest temperature testing, according to the author. The composites had a comparable stress–strain response to of that of PMMA. They demonstrated less strain softening in both quasi-static and intermediate strain rate tests, due to the particles impeding the polymer chains' mobility. Considering lower yield strength of Al than PMMA, the composites' strength dropped as the volume fraction of particles rose. This is due to a rule of mixtures effect. The author found that lowering particle size enhanced the composite strength, attributed to the increased surface area of smaller particles, which resulted in better matrix bonding and stress transmission.

Seo et al. [94] established that viscous flow behaviour is influenced by filler content, particle size, and temperature, as well as the density of filler particles inside the glass matrix. The researchers examined a glass composite made up of Bi_2O_3–B_2O_3–ZnO and fillers such as cordierite and willemite. With increasing filler content and density, the apparent viscosity of the glass composites rose. According to the study, the homogeneous distribution of the filler in the glass matrix results in improved wetting behaviour, which leads to increased fluidity and reduced viscosity. For both glass composites, the migration distance of fillers in the glass matrix increased when the sintering temperature was raised (Figure 15). The authors observed that as sintering progressed, the migration distance was determined by the density of the filler and the energy of the solid and liquid interfaces. The nonreactive and rigid character of the filler hampered the viscous flow of the willemite–glass composite. At the softening temperature, the increased density of willemite filler may cause a larger internal force within the glass matrix. This increased force causes

willemite filler particles to reorganise on the glass matrix's base, resulting in a flow gap in the willemite–glass composite.
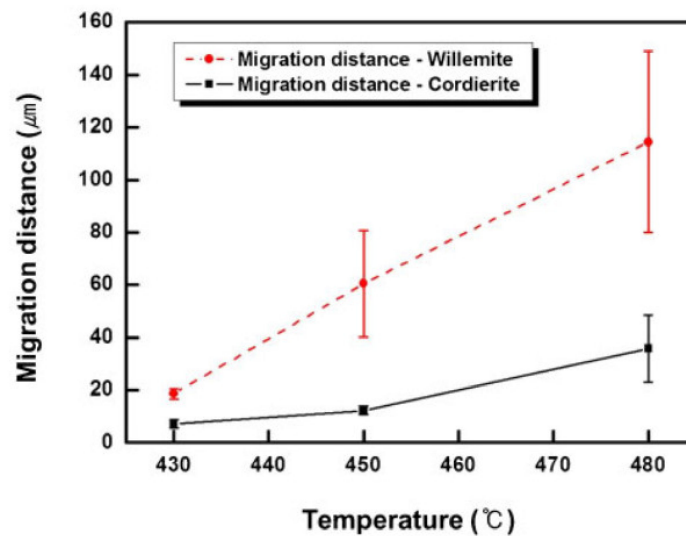
Figure 15. Migration distance of filler particles (cordierite, willemite, 10 vol. %, 11 μm) into the glass matrix upon sintering at 480 °C for 60 min at a heating rate of 10 °C min^{-1} (used with copyright permission) [94].

Samal et al. [95] also analysed the viscosities of the composites as a function of the size of the fillers (<20 wt. % of Al_2O_3, ZnO, and TiO_2) in a glass matrix: Bi_2O_3–B_2O_3–ZnO. The authors determined that when the filler content was high, the filler had no effect on the composite, but when the filler level was low to medium, the filler had a substantial impact on the behaviour of the composite. At higher firing temperatures, the viscous flow dominated wetting more in glass and less in the filler composite. It was found that with the increase in the fluidity, the viscosity lowered. The authors presented a relationship mechanism for various filler sizes in relation to glass contents, as illustrated in Figure 16. According to the mechanism, glass melted more easily when the filler particle size was larger than the parent glass particle size, and fluidity rose. Agglomeration was more likely in composites with smaller filler sizes. Due to high homogeneity between the filler and glass particles of the same sizes, the viscosity was relatively low with increasing fluidity.
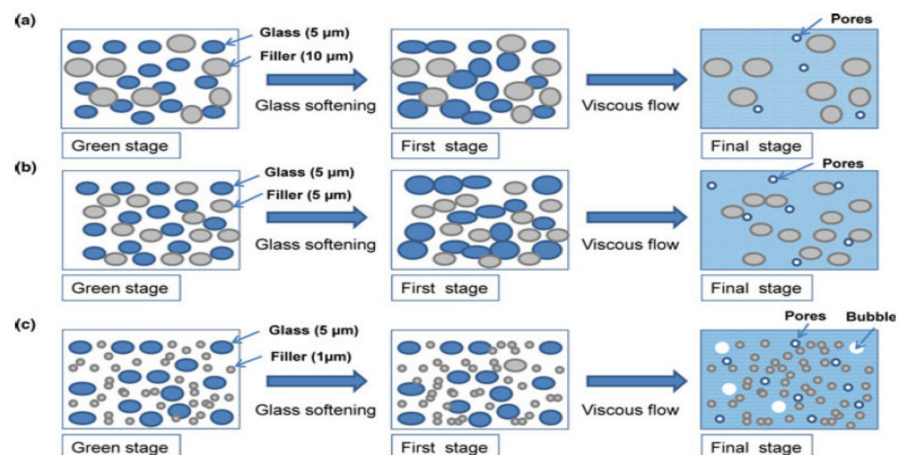
Figure 16. The mechanisms of the production of composites with varied particle sizes are depicted schematically. (**a**) Fillers with larger particles sizes (10 μm) than the glass particles (5 μm); (**b**) Same filler and glass particle sizes (5 μm); (**c**) Fillers with smaller particle sizes (1 μm) than the glass particles (5 μm) (used with copyright permission) [95].

Shin et al. [96] examined how the addition of crystalline TiO_2 and SiO_2 fillers to $BaO–ZnO–B_2O_3–SiO_2$ glass affected its characteristics. It was discovered that substituting SiO_2 for TiO_2 considerably lowered the dielectric constant while maintaining good optical reflectance and an adequate coefficient of thermal expansion when TiO_2 was employed alone. According to the results, SiO_2 addition with TiO_2 yielded 55% optical reflectance, a coefficient of thermal expansion of 8.3×10^{-6} K^{-1}, and a dielectric constant of about 7.5. It was found that all these parameters had great influence on barrier rib applications.

Lin et al. [97] examined how glassy polymer chains interact with homogeneously dispersed carbon nanotubes in nanocomposites made from surface-grafted multi-walled carbon nanotubes dispersed in two polymer systems, polystyrene and poly(phenylene oxide), which represent brittle and ductile polymers, respectively. Surface-grafted multi-walled carbon nanotubes distributed in a polymer matrix were shown to significantly toughen the glassy polymer by delocalising plastic flows caused by a substantial increase in chain friction during micro-deformation. The interactions between multi-walled carbon nanotubes and polymer chains are significantly different for crazes, forming polystyrene, and shear deformation zones, forming poly(phenylene oxide), according to the findings, which could be related to differences in the chain entanglement network topology. Multi-walled carbon nanotubes increased the chain friction in poly(phenylene oxide) nanoplastic flows, but it had no effect on the qualitative dependency of chain friction on the degree of drawing during flow. According to local stress analysis, entanglement network extensibility influences the mode of deformation that leads to crazing or shear yielding as well as the interaction between stretched chains and individual nanotubes.

Merkel et al. [97] discovered that the physical dispersion of non-porous, nanoscale, fumed silica particles in glassy amorphous poly(4-methyl-2-pentyne) simultaneously and surprisingly enhanced both membrane permeability and selectivity for large organic molecules over small permanent gases. These highly unusual property enhancements, in contrast to results obtained in conventional filled polymer systems, reflect the fumed silica-induced disruption of polymer chain packing and an accompanying subtle increase in the size of free volume elements through which molecular transport occurs. The distribution of fumed silica particles in poly(4-methyl-2-pentyne) is shown in the transmission electron microscopy (TEM) images presented in Figure 17, which reveals that the number of fumed silica particles, as well as their mean aggregate size, increases with fumed silica concentration.

Polinski [98] investigated the effects of a bimodal particle size distribution on the parameters including shear viscosity, dynamic viscosity, primary normal stress coefficient, and storage modulus of filled polymeric systems. It was demonstrated in the article that in comparison to the characteristics of composite systems with a unimodal size distribution of particles, all of these parameters were diminished. Furthermore, as the modality of the solids mixtures was raised, the maximum packing fraction rose. When the bimodal effects were integrated into the maximum packing parameter using Ouchiyama and Tanaka's approach [99], the decreases in rheological properties relative to the characteristics of the matrix fluid were efficiently represented.

Brouwers [100] examined polydisperse particle void fraction and geometric random packing. When the exponent (distribution modulus) of the power law function is 0, bimodal packing can be converted into a continuous particle-size distribution of the power law type. The distribution modulus was shown to be positive for maximal geometric packings comprising sieve fractions or separately sized particles. Additionally, the author provided a model to predict the polydisperse power law packing fraction. The model was solely influenced by the distribution exponent, size, mode of packing, and particle shape. For a number of particle shapes and their packing modes, these parameters are given. The packing fraction analytical expression is compared to experiments described in the literature and determined to be in excellent agreement.
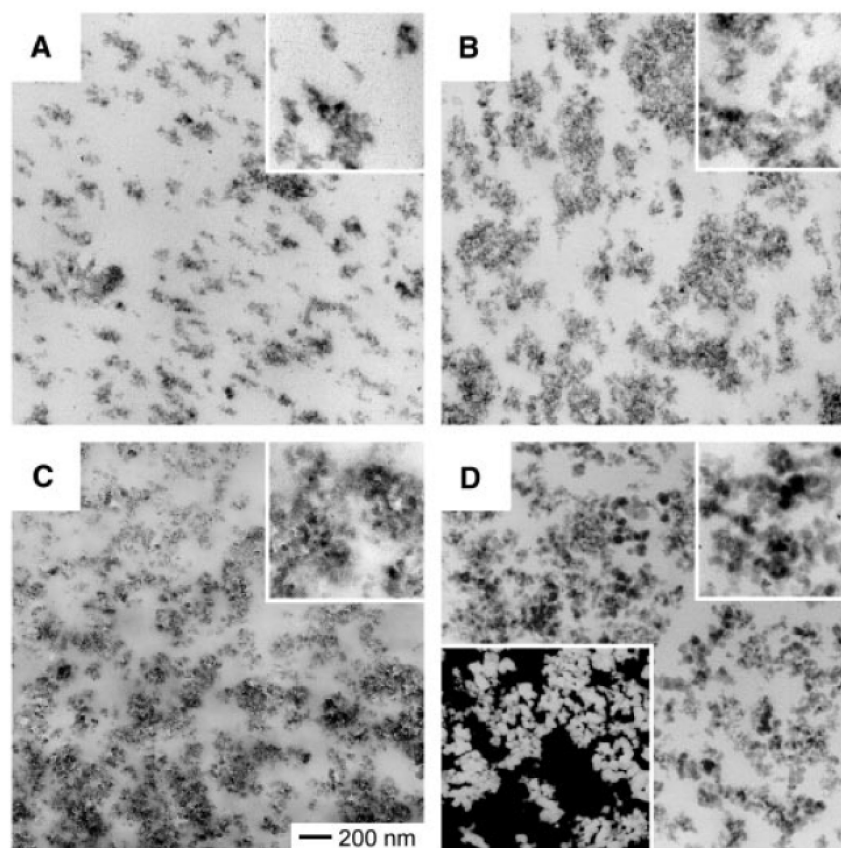
Figure 17. Energy-filtered TEM images of poly(4-methyl-2-pentyne) containing different concentrations (in wt. %/vol. %) of a hydrophobic fumed silica (TS-530): (**A**) 15/6, (**B**) 30/13, and (**C**) 40/19. (**D**) shows poly(4-methyl-2-pentyne) containing a hydrophilic fumed silica (L-90) at the same loading level as in (**C**) (used with copyright permission) [97].

The microstructure and dielectric characteristics of composites made up of polyvinylidene fluoride and calcium copper titanate particles were studied by Yang et al. [101]. The conductivity of the composite containing nanosized calcium copper titanate particles drops dramatically with rising temperature in the low-frequency range (100–104 Hz) and increases somewhat in the high-frequency range, according to the findings. Temperature has no effect on the conductivity of the composite containing microsized calcium copper titanate particles. Theoretical study further revealed that the dielectric performance of the composite containing nanosized calcium copper titanate particles defies traditional mixing principles, with the large dielectric constant owing mostly to interfacial polarisation. As the sizes of the calcium copper titanate particles were reduced from micro to nano, the interfacial effect was greatly improved, and interfacial polarisation became the important determinant, according to the findings.

4.4. Miscellaneous Applications of Glassy Polymers

Asai et al. [102] created a pressure-sensitive paint formulation using glassy poly [1–(trimethylsilyl)–1–propyne] as a binder for cryogenic and unstable wind-tunnel testing. This polymer has exceptionally high gas permeability. The authors showed that even at cryogenic temperatures, the created formulation-maintained oxygen sensitivity had a quick response time, and may be sprayed on any model surface, notably, stainless steel and ceramics. According to the studies, the developed coating was best suited to low-pressure applications due to its high quenching constant. A few milliseconds were the response time for a step change in pressure from vacuum to atmosphere. This coating can also be used in short-duration stress tunnel testing.

Loui et al. [103] designed a microcantilever-based sensor array that can detect a variety of chemical vapour analytes while being compact and low-power. The device worked by using the static deflection of piezoresistive cantilevers caused by the expansion of glassy polyolefin coatings during chemical vapour sorption. The polymers were chosen based on their Hildebrand solubility parameters to cover a wide range of chemical characteristics in order to maximise sensor sensitivity to various chemical analytes. Comparison of the polymer/vapor partition coefficient to the cantilever deflection responses revealed that, although general trends may be expected, a simple linear connection did not exist, highlighting the necessity for a functional model to characterise the chemical-to-mechanical transduction. It was also found that covalent bonding of the polymer coatings to the cantilever substrate may assist avoid creep and delamination in long-term deployment applications in humid or severe environments.

Hubmann et al. [104] used cellulose nanocrystals based on glassy polymers as an adhesive to produce UV-curable coatings. The authors grafted 3-isopropenyl-α,α-dimethylbenzyl isocyanate onto polyether-polyol-containing cellulose nanocrystals at loading levels of up to 1.8 wt.%. They found a 154% increase in adhesive strength and a 16% increase in tensile strength on average. The rapid transformation of a cellulose nanocrystals polyol solution into a high-viscosity photocurable prepolymer suspension, followed by the creation of a hydrogen-bonded network between the nanoparticles and the developing polymer matrix, was thought to be responsible for the results. When examining the fracture surfaces through scanning electron microscopy (SEM), the nanocomposites' capacity to undergo plastic deformation for energy dissipation was lowered, as illustrated in Figure 18. The roughness of the fracture surface rose considerably after integrating cellulose nanocrystals and new fracture characteristics along ramps appeared, possibly due to more recurrent crack front distortions. They concluded that the modest filler quantity employed is promising for applications where the presence of the filler should not significantly change optical or other thermo-mechanical characteristics. The decrease in internal tensions during UV-curing is most likely to be blamed for the improved adhesive characteristics.
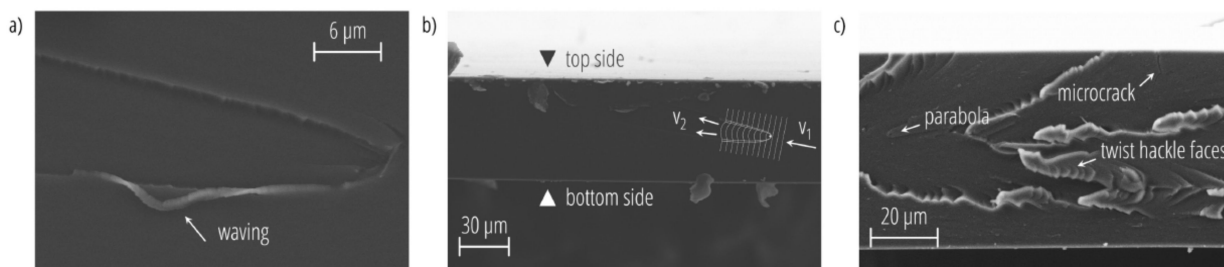
Figure 18. Selected SEM images of the fracture surfaces (**a**,**b**) in the absence of cellulose nanocrystals; (**c**) nanocomposite with 0.5 wt. % cellulose nanocrystals (used with copyright permissions) [104].

Viard et al. [105] synthesised two series of co-polymers with the general formula [B(C_2H_4 SiCH$_3$(NH)$_x$(NCH$_3$)$_y$)$_3$]$_n$, i.e., composed of B(C_2H_4SiCH$_3$NH)$_x$ and B(C_2H_4SiCH$_3$NCH$_3$)$_y$ (C_2H_4 = CHCH$_3$, CH$_2$CH$_2$) building blocks in a well-defined x:y ratio. They found that excessive methylamine addition resulted in co-polymers with more ending groups and, in particular, more tetracoordinated boron atoms, which are considered to play a key role in the precursors' meltspinnability. It was also observed that the excess methylamine addition is thought to result in the creation of polymer chains and therefore fewer rigid structures, allowing for improved chain mobility. According to the findings, due to the excess of methylamine, the chemical structure of the preceramic polymer may be fine-tuned to fit the melt-spinning criteria. Furthermore, the green fibres were found to be more effectively infusible by the ammonia curing procedure before being pyrolyzed under nitrogen at 1000 °C to produce Si–B–C–N ceramic fibres with reasonably high mechanical characteristics.

5. Physical Ageing in Glassy Polymers Coatings

For gas separations, several polymers have been investigated, but only a few membrane materials have made it to commercial usage, and this has not changed in decades, primarily due to physical ageing. Physical ageing is prevalent in glassy materials, in which a change in a property is seen as a function of storage time with no other external influences [106]. The phenomena are caused by the fact that they are typically out of equilibrium, and include a wide variety of characteristics, including bulk properties such as specific volume, enthalpy, mechanical, and dielectric response, as well as molecular properties such as the free volume distribution [107]. According to the latest research, super-glassy polymer materials age in two stages: rapid densification occurs within the first few days, followed by a progressive rearranging of packed chains over longer time periods toward a theoretical equilibrium state. It is crucial to keep in mind that physical ageing only comprises reversible changes in characteristics, not structural alterations. Physical ageing distinguishes itself from other variables that can affect characteristics over time, such as chemical ageing, degradation, absorption, or contamination.

Pfromm and Koros [108] highlighted the fact that membrane thickness affects ageing. In thin films made of a fluorinated polyimide and polysulfone, the physical ageing of polysulfone was accelerated, which was ascribed to free volume diffusion. This process appeared to be more rapid as the film thickness lowered, driven by the rising segment mobility in the vicinity of a free surface [109]. Chung et al. [110] investigated the ageing of different asymmetric and composite membranes, and found that the rate of ageing was affected by spinning circumstances, such as shear rates.

Huang and Paul [71] examined the influence of physical ageing on gas permeability in free-standing thin polymer sheets. Thin polysulfone films with thicknesses of 400–1000 nm were obtained using both solution-casting and spin-coating techniques. When thin films were heated above T_g, the contraction caused by molecular chain relaxation resulted in a substantial thickness increase, as shown in Figure 19. These films demonstrated a considerable drop in gas permeability as a result of a free volume decrease during storage in the glassy phase. Physical ageing occurred at a pace that was several orders of magnitude more rapid than that found in bulk films.
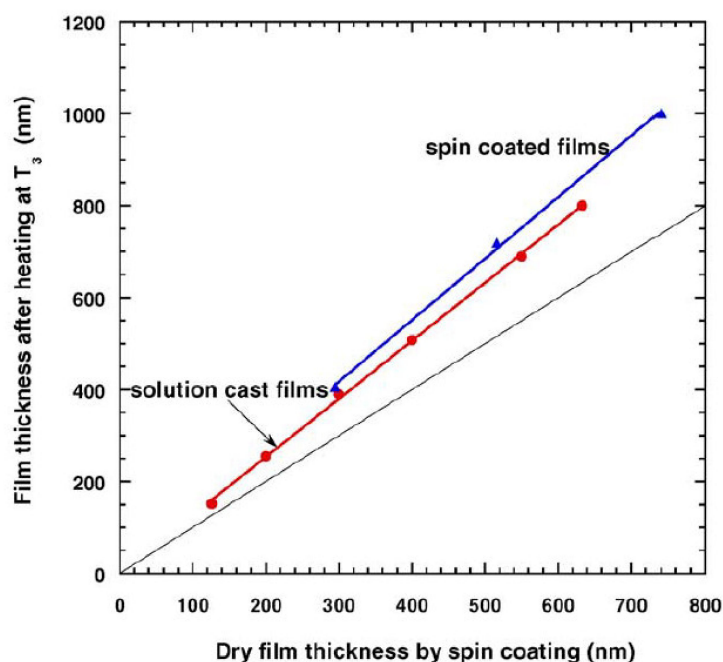
Figure 19. Final thicknesses of polysulfone thin films after heating above T_g (used with copyright permission) [71].

McCaig and Paul [111] also evaluated physical ageing on the basis of thickness and how ageing time affected the gas permeation characteristics of films produced from bisphenol-A benzophenone dicarboxylic acid glassy polyarylate. Physical ageing was responsible for a considerable drop in gas permeability over time after quenching the polymer from above its glass transition temperature and the rate of change was faster for thinner films. The permeability decreased and selectivity increased with ageing time. The ageing process was shown to be reversed by heating above the T_g, as illustrated in Figure 20.
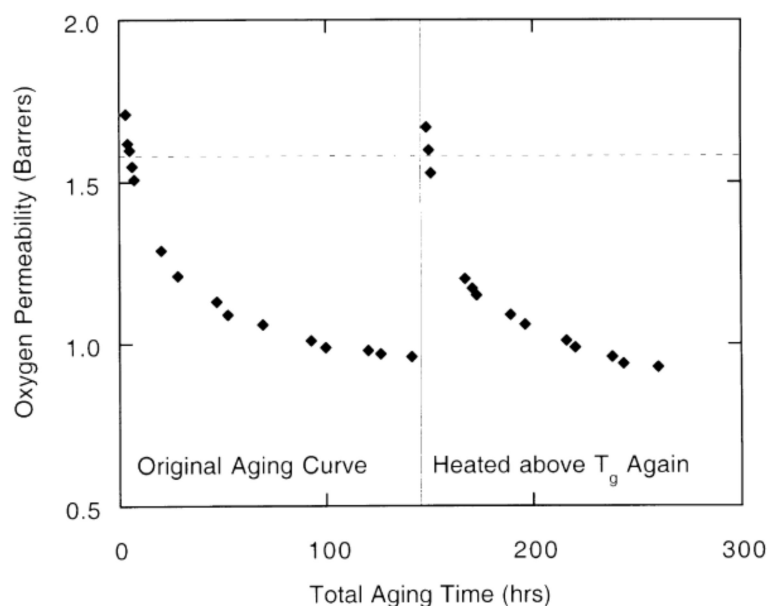
Figure 20. Demonstration of the reversal of the ageing effects on O_2 permeability coefficients by heating above T_g again. The vertical line marks the time when the membrane was re-heated above T_g (used with copyright permission) [111].

Kim et al. [112] measured the permeability of N_2, O_2, He, CH_4, and CO_2 in thin films of crosslinked and uncrosslinked 6FDA-based polyimides containing DABA units in the chain as a function of ageing time at 35 °C. Physical ageing reduced the permeability of these thin films while significantly increasing their selectivity for each polymer structure. The permeability of crosslinked polyimides was substantially lower than that of uncrosslinked polyimides. Depending on the polymer structure, oxygen permeability reduced by two to three times after roughly 2000 h of ageing. Crosslinked polyimide films appeared to have somewhat greater or similar ageing rates to uncrosslinked polyimide films. The self-impeding kinetic model suggested by Struik [113] accurately described the fractional free volume findings for a given film thickness.

Xia et al. [114] investigated the ageing of a polyimide—Matrimid—in the form of thin films in both pure gas and CO_2–CH_4 (or CO_2–N_2) mixed gas permeation. The effect of pressure on pure gas permeability, according to the authors, suggested that physical ageing affects both Henry's law and the Langmuir term in the dual-mode sorption model. It was also found that the Langmuir sorption declined considerably more rapidly in thin films as compared to the thick films. As the thickness of Matrimid films was lowered to the range necessary to construct high flux commercial asymmetric membranes, and as the ageing period increased, the films became more susceptible to CO_2 plasticization. For CO_2/N_2 feed mixtures, the combined effect of CO_2 plasticization and competitive sorption/permeation on thin Matrimid films appeared to be less substantial than for CO_2/CH_4 feed mixtures. In another study, Xia et al. [115] assessed thin films composed of polyetherimide for their gas permeability and found the same ageing pattern. Thin films had a higher permeability

than thick films at first, but their permeability gradually declined until it was considerably below that of the thick film.

Tiwari et al. [116] also investigated the physical ageing of PIM-1 by measuring changes in pure gas permeability of O_2, N_2, and CH_4 at 35 °C. They discovered that thin PIM-1 films aged faster than thick films with relative permeability for thin PIM-1 films, decreasing by 67% after 1000 h of ageing compared to 53% for thick films. The influence of casting solvent's vapour pressure and boiling point on the ageing and selectivity of thin films was more evident, with initial permeability nearly two times greater for films cast with chloroform ($CHCl_3$) than for those cast with ortho-dichlorobenzene (o-DCB). For thick films, the influence of the casting solvent on the initial permeability was less pronounced. With increasing sorption temperature, the Henry's law constant increased, which was connected to the thin layer being less deep in the glassy state at higher sorption temperatures. High CO_2 pressure enhances diffusivity and decreases solubility at a constant ageing period, which supports a rise in free volume and severe plasticization in PIM-1 thin films.

Physical ageing was measured by Huang and Paul [117] by evaluating the changes in the refractive indexes of thin films made of three glassy polymers: polysulfone, polyimide, and polycarbonate (2,6-dimethyl-1,4-phenylene oxide). The Lorentz–Lorenz equation, shown below, was used to calculate isothermal volumetric ageing rate, r, and also to give the relationship between changes in refractive index and densification (or volume relaxation) over time.

$$r = \left(\frac{\partial \ln \rho}{\partial \ln t} \right)_{P,T} = \left(\frac{\partial \ln L}{\partial \ln t} \right)_{P,T} = \left(\frac{\partial \log L}{\partial \log t} \right)_{P,T} \tag{21}$$

The volumetric ageing rate was found to be dependent on the polymer structure and film thickness. Physical ageing caused the refractive index in various forms to rise more or less linearly with log t during the densification process. The more accelerated ageing of thin films than bulk polymers had been suggested in the literature to be due to the diffusion of free volume to the film's surface, analogous to the diffusion of abnormalities, leading ageing to be thickness-dependent.

Drozdov [118] created a model for the influence of physical ageing on amorphous glassy polymers' linear viscoelastic response. In tensile relaxation tests and torsional dynamic testing at various temperatures, the author used stress–strain relationships to match experimental data for poly(methyl methacrylate), poly(styrene-co-acronitrile), and poly(vinyl acetate). According to the findings, increased annealing temperature caused an increase in the rate of relaxation while decreasing the apparent rate of structural recovery. The notion of cooperative relaxation was combined with the coarsening concept for structural recovery to provide constitutive equations. The author found that for the approximation of experimental data in mechanical testing on aged specimens, the time-ageing time concept of superposition was not required. It was also shown that there was great consistency between observations and numerical simulation findings when the relaxation rate was independent of waiting time, but the average energy and specific stiffness of a cooperatively rearranged regions rose two-fold. It was also discovered that the annealing temperature T had a significant impact on energy landscape reformation. An increase in the apparent rate of ageing was caused by an increase in the degree of supercooling. It had a far smaller influence on the development of initial elastic moduli.

Yong et al. [119] used polyhedral oligomeric silsesquioxane–POSS nanoparticles to provide a straightforward method for increasing the CO_2 permeability of PIM-1 without affecting its selectivity while also suppressing ageing. At low particle loadings, the nanoparticles improved gas diffusivity, but at large particle loadings, they caused chain rigidification. The optimum gas-separation characteristics may be achieved with just 2% POSS nanoparticles in PIM-1. The POSS nanoparticles disturbed chain packing at low loadings and caused chain rigidification at high loadings, according to positron annihilation lifetime spectroscopy data. The authors found that POSS nanoparticles decreased physical ageing over 120 days when compared to PIM-1. The results showed that the permeability

of the PIM-1/POSS (98:2) membrane was greater, and the physical ageing rate was lower. This was due to the fact that implanted hard POSS nanoparticles may stiffen and delay the segmental motion of PIM-1 polymeric chains.

6. Conclusions

This review is hoped to lead to a better understanding of glassy polymer systems' behaviour throughout processes including diffusion, sorption and physical ageing. The literature on glassy polymers may be categorised as follows:

- Sufficient literature is available on diffusion in glassy polymers. Models of diffusion in glassy polymers are governed by Fickian and non-Fickian diffusion, out of which non-Fickian is more common in glassy polymers. The characteristics of the diffusants, the polymer network, and the solvents all have a role in diffusion. When a penetrant is a gas at the required temperature, predicting volumetric behaviour for the glassy–polymer–penetrant system becomes more challenging. However, none of the available models are uniformly applicable in all cases for the entire drying process. Furthermore, comparative studies of various models are missing in the literature;

- The properties of glassy polymers are dependent on sorption isotherms, and to explain the sorption in glassy polymers, there are various models explored in the literature [43–45,47,49,50,53,59,63]. The dual-mode sorption model, which is based on sorption sites that obey Henry's law dissolution and Langmuir-type sorption; the GAB model, which is an extension of the BET method for multilayer adsorption of small molecules in a solid adsorbent; and the NET-GP model, which was developed after investigating non-Fickian diffusion in glassy polymers and molecular simulation techniques, have all been reviewed in this work;

- Characteristics of glassy polymers are dependent on diffusion and sorption; therefore, there is a need for an extension and modification of existing models. There are limitations to the use of physical models, and further research is needed to generalise the models which can be executed efficiently. Machine learning techniques appear to be extremely promising for developing diffusion and sorption models, and they should be further investigated;

- Glassy polymer coatings have wide applications, including membrane separation, drug delivery systems, corrosion prevention, and many more which have been explained in this review. Use of multicomponent coatings, such as binary and tertiary coatings, along with materials such as surfactants, nanoparticles which enhance the properties of glassy polymers need to be explored. The area of green synthesis and biodegradable glassy polymers also needs to be explored to make the applications more environmentally friendly;

- Despite having so many applications, there is still a challenge for current researchers to simulate real-life coating problems due to issues such as physical ageing which have briefly been described in the review. There is still a scope to explore those glassy polymers which are more durable against physical ageing. Emphasis should be given to the crosslinking of glassy polymers because they are effective against physical ageing.

Conflicts of Interest: The authors declare no conflict of interest.

Nomenclature

a	penetrant activity in a polymer in the GAB model, dimensionless
A	temperature-dependent constant in the GAB model, dimensionless
A_0	pre-exponential factor of a temperature-dependent constant in the GAB model, dimensionless
A'	temperature-dependent constant in the new dual-mode sorption model, dimensionless
b	the Langmuir hole affinity parameter, atm^{-1}
C	the total gas concentration in a glassy polymer, cm^3/cm^3 polymer
C_D	the gas concentration based on Henry's law sorption, cm^3/cm^3 polymer
C_H	the gas concentration based on Langmuir sorption, cm^3/cm^3 polymer
C'_H	the capacity parameter, cm^3/cm^3
C_p	monolayer sorption capacity, dimensionless
$\overline{C_p}$	weighted mean value of polymer sorption capacity to sorbate molecules, dimensionless
D_{01}	pre-exponential factor independent of temperature, m$^2 \cdot$s^{-1}
D	binary diffusion coefficient, m$^2 \cdot$s^{-1}
D_1	solvent self-diffusion coefficient, m$^2 \cdot$s^{-1}
D_s	thermodynamic diffusion coefficient for solute mass flux in the solute–polymer mixture, m$^2 \cdot$s^{-1}
H_L	heat of condensation of a pure vapor, Kcal/gmol
H_m	heat of sorption of monolayer of a vapor, Kcal/gmol
H_n	heat of sorption of multi-molecular layers of a vapor, Kcal/gmol
j_s	diffusive solute flux in the solute-polymer mixture, Kg$\cdot$m^{2}s^{-1}
k	temperature-dependent constant in the GAB model, dimensionless
Kg	mass transfer coefficient at the coating-air interface (kg$\cdot$m^{-2} s$^{-1} \cdot$atm^{-1})
K_0	pre-exponential factor of a temperature-dependent constant in the GAB model, dimensionless
k'	temperature-dependent constant in the new DMS model, dimensionless
k_D	the Henry's law coefficient, cm^3/cm$^3 \cdot$atm
L	Lorentz–Lorenz parameter, dimensionless
p	applied gas pressure, atm
P	pressure, atm
p_1^*	characteristic pressure of pure component 1, atm
p_2^*	characteristic pressure of pure component 2, atm
R	gas constant, Jmol$^{-1} \cdot$K^{-1}
r_1^0	number of lattice sites occupied by a mole of pure component 1, dimensionless
T	temperature, K
T_g	glass transition temperature, K
T_1^*	characteristic temperature of pure component 1, K
u_1	solvent volume fraction, dimensionless
$\hat{V}_2^*$	specific hole-free volume for a diffusional step of component 2, m^3/kg
v_i^*	volume occupied by a mole of lattice sites of pure substance, cm^3
$\hat{V}_{FH_2}^*$	the specific hole-free volume, m^3/Kg
x_∞	solvent mole fraction at the air phase (bulk)

Greek Letters

μ_s^{NE}	nonequilibrium solute chemical potential in the solute–polymer mixture, J$\cdot$kg^{-1}
μ_1	solvent chemical potential, J$\cdot$kg^{-1}
ρ_s	solute mass per unit volume in the solute–polymer mixture, kg$\cdot$m^{-3}
ρ_p	polymer mass per unit volume in the solute–polymer mixture, kg$\cdot$m^{-3}
ρ	density of the polymer, kg$\cdot$m^{-3}
ρ_2^*	characteristic density of pure component 2, kg$\cdot$m^{-3}
φ_i	van der Waals volume fractions of the group "i" in the polymer matrix, dimensionless
ω_s	solute mass fraction in the solute–polymer mixture, dimensionless

References

1. Sharma, J.; Ahuja, S.; Arya, R.K. Effect of molecular weight on morphology and thermal properties of poly (styrene)-poly (methyl methacrylate)-ethylbenzene coatings. *Prog. Org. Coat.* **2019**, *132*, 468–474. [CrossRef]
2. Auras, R.; Harte, B.; Selke, S. An overview of polylactides as packaging materials. *Macromol. Biosci.* **2004**, *4*, 835–864. [CrossRef] [PubMed]
3. Bergström, J.S.; Hayman, D. An overview of mechanical properties and material modeling of polylactide (PLA) for medical. *Ann. Biomed. Eng.* **2016**, *44*, 330–340. [CrossRef]
4. Srinivasan, R.; Auvil, S.R.; Burban, P.M. Elucidating the mechanism(s) of gas transport in poly[1-(trimethylsilyl)-1-propyne] (PTMSP) membranes. *J. Membr. Sci.* **1994**, *86*, 67–86. [CrossRef]
5. Ichiraku, Y.; Stern, S.A.; Nakagawa, T. An investigation of the high gas permeability of poly (1-Trimethylsilyl-1-Propyne). *J. Membr. Sci.* **1987**, *34*, 5–18. [CrossRef]
6. Zeng, M.; Feng, Z.; Huang, Y.; Liu, J.; Ren, J.; Xu, Q.; Fan, L. Chemical structure and remarkably enhanced mechanical properties of chitosan-graft-poly(acrylic acid)/polyacrylamide double-network hydrogels. *Polym. Bull.* **2017**, *74*, 55–74. [CrossRef]
7. Morisato, A.; Pinnau, I. Synthesis and gas permeation properties of poly(4-methyl-2-pentyne). *J. Membr. Sci.* **1996**, *121*, 243–250. [CrossRef]
8. Budd, P.M.; Elabas, E.S.; Ghanem, B.S.; Makhseed, S.; McKeown, N.B.; Msayib, K.J.; Tattershall, C.E.; Wang, D. Solution-processed, organophilic membrane derived from a polymer of intrinsic microporosity. *Adv. Mater.* **2004**, *16*, 456–459. [CrossRef]
9. Robeson, L.M.; Liu, Q.; Freeman, B.D.; Paul, D.R. Comparison of transport properties of rubbery and glassy polymers and the relevance to the upper bound relationship. *J. Membr. Sci.* **2015**, *476*, 421–431. [CrossRef]
10. Hadj Romdhane, I.; Price, P.E.; Miller, C.A.; Benson, P.T.; Wang, S. Drying of glassy polymer films. *Ind. Eng. Chem. Res.* **2001**, *40*, 3065–3075. [CrossRef]
11. Vrentas, J.; Duda, J. Diffusion in polymer–solvent systems. I. Reexamination of the free-volume theory. *J. Polym. Sci. Polym. Phys. Ed.* **1977**, *15*, 403–416. [CrossRef]
12. Vrentas, J.; Duda, J. Diffusion in polymer–solvent systems. II. A predictive theory for the dependence of diffusion coefficients on temperature, concentration, and molecular weight. *J. Polym. Sci. Polym. Phys. Ed.* **1977**, *15*, 417–439. [CrossRef]
13. Yapel, R.A. A Physical Model of the Drying of Coated Films. Master's Thesis, University of Minnesota, Minneapolis, MN, USA, 1988.
14. Alsoy, S.; Duda, J. Drying of solvent coated polymer films. *Dry. Technol.* **1998**, *16*, 15–44. [CrossRef]
15. Alsoy, S. Predicting drying in multiple-zone ovens. *Ind. Eng. Chem. Res.* **2001**, *40*, 2995–3001. [CrossRef]
16. Schabel, W.; Scharfer, P.; Kind, M. Measurement and simulation of concentration profiles during drying of thin films with help of confocal-micro-raman spectroscopy. *Chem. Ing. Tech.* **2003**, *75*, 1105–1106. [CrossRef]
17. Schabel, W.; Scharfer, P.; Muller, M.; Ludwig, I.; Kind, M. Measurement and simulation of concentration profiles in the drying of binary polymer solutions. *Chem. Ing. Tech.* **2003**, *75*, 1336–1344. [CrossRef]
18. Scharfer, P.; Schabel, W.; Kind, M. Modelling of alcohol and water diffusion in fuel cell membranes—Experimental validation by means of in situ Raman spectroscopy. *Chem. Eng. Sci.* **2008**, *63*, 4676–4684. [CrossRef]
19. Arya, R.K. Measurement of concentration profiles in thin film binary polymer-solvent coatings using confocal Raman spectroscopy: Free volume model validation. *Dry. Technol.* **2014**, *32*, 992–1002. [CrossRef]
20. Arya, R.K.; Vinjamur, M. Measurement of concentration profiles using confocal Raman spectroscopy in multicomponent polymeric coatings—Model validation. *J. Appl. Polym. Sci.* **2013**, *128*, 3906–3918. [CrossRef]
21. Siebel, D.; Scharfer, P.; Schabel, W. Prediction of diffusion in a ternary solvent–solvent–polymer blend by means of binary diffusion data: Comparison of experimental data and simulative results. *J. Appl. Polym. Sci.* **2016**, *133*, 43899. [CrossRef]
22. Zhang, C.; Cappleman, B.; Defibaugh-Chavez, M.; Weinkauf, D. Glassy polymer-sorption phenomena measured with a quartz crystal microbalance technique. *J. Polym. Sci. Part. B Polym. Phys.* **2003**, *41*, 2109–2118. [CrossRef]
23. Masaro, L.; Zhu, X.X. Physical models of diffusion for polymer solutions, gels and solids. *Prog. Polym. Sci.* **1999**, *24*, 731–775. [CrossRef]
24. Grinsted, R.A.; Clark, L.; Koenig, J.L. Study of cyclic sorption-desorption into poly(methyl methacrylate) rods using NMR imaging. *Macromolecules* **1992**, *25*, 1235–1241. [CrossRef]
25. Weisenberger, L.A.; Koenig, J.L. NMR imaging of diffusion processes in polymers: Measurement of the spatial dependence of solvent mobility in partially swollen PMMA rods. *Macromolecules* **1990**, *23*, 2445–2453. [CrossRef]
26. Vrentas, J.S.; Vrentas, C.M. Volumetric behavior of glassy polymer-penetrant systems. *Macromolecules* **1989**, *22*, 2264–2266. [CrossRef]
27. Vrentas, J.S.; Duda, J.L.; Ling, H.C. Antiplasticization and volumetric behavior in glassy polymers. *Macromolecules* **1988**, *21*, 1470–1475. [CrossRef]
28. Laksmana, F.L.; Hartman Kok, P.J.A.; Vromans, H.; Van der Voort Maarschalk, K. Predicting the diffusion coefficient of water vapor through glassy HPMC films at different environmental conditions using the free volume additivity approach. *Eur. J. Pharm. Sci.* **2009**, *37*, 545–554. [CrossRef]
29. Duda, J.L.; Hadj Romdhane, I.; Danner, R.P. Diffusion in glassy polymers—Relaxation and antiplasticization. *J. Non-Cryst. Solids* **1994**, *172*, 715–720. [CrossRef]
30. Vrentas, J.S.; Duda, J.L. Molecular diffusion in polymer solutions. *AIChE J.* **1979**, *25*, 1–24. [CrossRef]

31. Wang, B.-G.; Yamaguchi, T.; Nakao, S.-I. Solvent diffusion in amorphous glassy polymers. *J. Polym. Sci. Part. B Polym. Phys.* **2000**, *38*, 846–856. [CrossRef]

32. Verros, G.D. Application of irreversible thermodynamics to the solvent diffusion in an amorphous glassy polymer: A comprehensive model for drying of toluene-poly(methyl methacrylate) coatings. *Can. J. Chem. Eng.* **2015**, *93*, 2298–2306. [CrossRef]

33. Powers, G.W.; Collier, J.R. Experimental modeling of solvent-casting thin polymer films. *Polym. Eng. Sci.* **1990**, *30*, 118–123. [CrossRef]

34. Arya, R.K. Finite element solution of coupled-partial differential and ordinary equations in multicomponent polymeric coatings. *Comput. Chem. Eng.* **2013**, *50*, 152–183. [CrossRef]

35. Sharma, J.; Arya, R.K.; Verros, G.D. A unified model for the drying of glassy polymer coatings. *Prog. Org. Coat.* **2019**, *134*, 219–225. [CrossRef]

36. Alsoy, S.; Duda, J.L. Modeling of multicomponent drying of polymer films. *AIChE J.* **1999**, *45*, 896–905. [CrossRef]

37. Sharma, J.; Kumar Arya, R.; Verros, G.D. A comprehensive model for the drying of glassy polymer coatings: The low solvent concentration area of the system poly(styrene)/P-xylene. *Prog. Org. Coat.* **2019**, *135*, 622–628. [CrossRef]

38. Davis, E.M.; Minelli, M.; Giacinti Baschetti, M.; Elabd, Y.A. Non-fickian diffusion of water in polylactide. *Ind. Eng. Chem. Res.* **2013**, *52*, 8664–8673. [CrossRef]

39. Tomba, J.P.; Arzondo, L.M.; Carella, J.M.; Pastor, J.M. Liquid-glassy polymer diffusion: Effects of liquid molecular weight and temperature. *Macromol. Chem. Phys.* **2007**, *208*, 1110–1121. [CrossRef]

40. Gallyamov, M.O. Sharp diffusion front in diffusion problem with change of state. *Eur. Phys. J. E* **2013**, *36*, 92. [CrossRef]

41. Santos, M.C.; Bendiksen, B.; Elabd, Y.A. Diffusion of liquid water in free-standing polymer films using pressure-contact time-resolved fourier transform infrared attenuated total reflectance spectroscopy. *Ind. Eng. Chem. Res.* **2017**, *56*, 3464–3476. [CrossRef]

42. Chern, R.T.; Koros, W.J.; Sanders, E.S.; Yui, R. "Second component" effects in sorption and permeation of gases in glassy polymers. *J. Membr. Sci.* **1983**, *15*, 157–169. [CrossRef]

43. Tsujita, Y. Gas sorption and permeation of glassy polymers with microvoids. *Prog. Polym. Sci.* **2003**, *28*, 1377–1401. [CrossRef]

44. Vieth, W.R.; Tam, P.M.; Michaels, A.S. Dual sorption mechanisms in glassy polystyrene. *J. Colloid Interface Sci.* **1966**, *22*, 360–370. [CrossRef]

45. Paul, D.R. Gas sorption and transport in glassy polymers. *Ber. Bunsenges. Phys. Chem.* **1979**, *83*, 294–302. [CrossRef]

46. Ricci, E.; De Angelis, M.G. Modelling mixed-gas sorption in glassy polymers for CO_2 removal: A sensitivity analysis of the dual mode sorption model. *Membranes* **2019**, *9*, 8. [CrossRef]

47. Saberi, M.; Rouhi, P.; Teimoori, M. Estimation of dual mode sorption parameters for CO_2 in the glassy polymers using group contribution approach. *J. Membr. Sci.* **2020**, *595*, 117481. [CrossRef]

48. Velioğlu, S.; Tantekin-Ersolmaz, S.B. Prediction of gas permeability coefficients of copolyimides by group contribution methods. *J. Membr. Sci.* **2015**, *480*, 47–63. [CrossRef]

49. Feng, H. Modeling of vapor sorption in glassy polymers using a new dual mode sorption model based on multilayer sorption theory. *Polymer* **2007**, *48*, 2988–3002. [CrossRef]

50. Timmermann, E.O. A BET-like three sorption stage isotherm. *J. Chem. Soc. Faraday Trans. 1 Phys. Chem. Condens. Phases* **1989**, *85*, 1631–1645. [CrossRef]

51. Vopička, O.; Friess, K. Analysis of gas sorption in glassy polymers with the GAB model: An alternative to the dual mode sorption model. *J. Polym. Sci. Part. B Polym. Phys.* **2014**, *52*, 1490–1495. [CrossRef]

52. Carlà, V.; Hussain, Y.; Grant, C.; Sarti, G.C.; Carbonell, R.G.; Doghieri, F. Modeling sorption kinetics of carbon dioxide in glassy polymeric films using the nonequilibrium thermodynamics approach. *Ind. Eng. Chem. Res.* **2009**, *48*, 3844–3854. [CrossRef]

53. Scherillo, G.; Galizia, M.; Musto, P.; Mensitieri, G. Water sorption thermodynamics in glassy and rubbery polymers: Modeling the interactional issues emerging from FTIR spectroscopy. *Ind. Eng. Chem. Res.* **2013**, *52*, 8674–8691. [CrossRef]

54. Doghieri, F.; Sarti, G.C. Nonequilibrium lattice fluids: A predictive model for the solubility in glassy polymers. *Macromolecules* **1996**, *29*, 7885–7896. [CrossRef]

55. Panayiotou, C.; Pantoula, M.; Stefanis, E.; Tsivintzelis, I.; Economou, I.G. Nonrandom hydrogen-bonding model of fluids and their mixtures. 1. Pure fluids. *Ind. Eng. Chem. Res.* **2004**, *43*, 6592–6606. [CrossRef]

56. Minelli, M.; Campagnoli, S.; De Angelis, M.G.; Doghieri, F.; Sarti, G.C. Predictive model for the solubility of fluid mixtures in glassy polymers. *Macromolecules* **2011**, *44*, 4852–4862. [CrossRef]

57. Sanchez, I.C.; Lacombe, R.H. An elementary molecular theory of classical fluids. Pure fluids. *J. Phys. Chem.* **1976**, *80*, 2352–2362. [CrossRef]

58. Galizia, M.; De Angelis, M.G.; Sarti, G.C. Sorption of hydrocarbons and alcohols in addition-type poly(trimethyl silyl norbornene) and other high free volume glassy polymers. II: NELF model predictions. *J. Membr. Sci.* **2012**, *405*, 201–211. [CrossRef]

59. Van der Vegt, N.F.A.; Briels, W.J.; Wessling, M.; Strathmann, H. The sorption induced glass transition in amorphous glassy polymers. *J. Chem. Phys.* **1999**, *110*, 11061–11069. [CrossRef]

60. Kirchheim, R. Sorption and partial molar volume of small molecules in glassy polymers. *Macromolecules* **1992**, *25*, 6952–6960. [CrossRef]

61. Spyriouni, T.; Boulougouris, G.C.; Theodorou, D.N. Prediction of Sorption of CO2 in Glassy Atactic Polystyrene at Elevated Pressures Through a New Computational Scheme. *Macromolecules* **2009**, *42*, 1759–1769. [CrossRef]

62. Boulougouris, G.C.; Economou, I.G.; Theodorou, D.N. On the calculation of the chemical potential using the particle deletion scheme. *Mol. Phys.* **1999**, *96*, 905–913. [CrossRef]

63. Neyertz, S.; Brown, D. Single- and mixed-gas sorption in large-scale molecular models of glassy bulk polymers. Competitive sorption of a binary CH_4/N_2 and a ternary $CH_4/N_2/CO_2$ mixture in a polyimide membrane. *J. Membr. Sci.* **2020**, *614*, 118478. [CrossRef]

64. Stubbs, J.M.; Chen, B.; Potoff, J.J.; Siepmann, J.I. Monte Carlo calculations for the phase equilibria of alkanes, alcohols, water, and their mixtures. *Fluid Phase Equilibria* **2001**, *183–184*, 301–309. [CrossRef]

65. Vergadou, N.; Theodorou, D.N. Molecular modeling investigations of sorption and diffusion of small molecules in glassy polymers. *Membranes* **2019**, *9*, 98. [CrossRef]

66. Kamiya, Y.; Bourbon, D.; Mizoguchi, K.; Naito, Y. Sorption, dilation, and isothermal glass transition of poly(ethyl methacrylate)-organic gas systems. *Polym. J.* **1992**, *24*, 443–449. [CrossRef]

67. Vrentas, J.S.; Vrentas, C.M. Hysteresis effects for sorption in glassy polymers. *Macromolecules* **1996**, *29*, 4391–4396. [CrossRef]

68. Fleming, G.K.; Koros, W.J. Dilation of polymers by sorption of carbon dioxide at elevated pressures. 1. Silicone rubber and unconditioned polycarbonate. *Macromolecules* **1986**, *19*, 2285–2291. [CrossRef]

69. Hölck, O.; Heuchel, M.; Böhning, M.; Hofmann, D. Simulation of experimentally observed dilation phenomena during integral gas sorption in glassy polymers. *J. Polym. Sci. Part B Polym. Phys.* **2008**, *46*, 59–71. [CrossRef]

70. Björklund, S.; Kocherbitov, V. Water vapor sorption-desorption hysteresis in glassy surface films of mucins investigated by humidity scanning QCM-D. *J. Colloid Interface Sci.* **2019**, *545*, 289–300. [CrossRef] [PubMed]

71. Huang, Y.; Paul, D.R. Experimental methods for tracking physical aging of thin glassy polymer films by gas permeation. *J. Membr. Sci.* **2004**, *244*, 167–178. [CrossRef]

72. Hoare, T.R.; Kohane, D.S. Hydrogels in drug delivery: Progress and challenges. *Polymer* **2008**, *49*, 1993–2007. [CrossRef]

73. Good, W.R. Diffusion of water soluble drugs from initially dry hydrogels. *Polym. Deliv. Syst.* **1976**, *5*, 139–156.

74. Lee, P.I. Novel approach to zero-order drug delivery via immobilized nonuniform drug distribution in glassy hydrogels. *J. Pharm. Sci.* **1984**, *73*, 1344–1347. [CrossRef]

75. El-Hag Ali Said, A. Radiation synthesis of interpolymer polyelectrolyte complex and its application as a carrier for colon-specific drug delivery system. *Biomaterials* **2005**, *26*, 2733–2739. [CrossRef] [PubMed]

76. Abou Taleb, M.F.; Abdel-Aal, S.E.; El-Kelesh, N.A.; Hegazy, E.-S.A. Adsorption and controlled release of Chlortetracycline HCl by using multifunctional polymeric hydrogels. *Eur. Polym. J.* **2007**, *43*, 468–477. [CrossRef]

77. Mazied, N.A.; Ismail, S.A.; Abou Taleb, M.F. Radiation synthesis of poly[(dimethylaminoethyl methacrylate)-co-(ethyleneglycol dimethacrylate)] hydrogels and its application as a carrier for anticancer delivery. *Radiat. Phys. Chem.* **2009**, *78*, 899. [CrossRef]

78. Mullarney, M.P.; Seery, T.A.P.; Weiss, R.A. Drug diffusion in hydrophobically modified N,N-dimethylacrylamide hydrogels. *Polymer* **2006**, *47*, 3845–3855. [CrossRef]

79. Rudzinski, W.E.; Chipuk, T.; Dave, A.M.; Kumbar, S.G.; Aminabhavi, T.M. PH-sensitive acrylic-based copolymeric hydrogels for the controlled release of a pesticide and a micronutrient. *J. Appl. Polym. Sci.* **2003**, *87*, 394–403. [CrossRef]

80. Brazel, C.S.; Peppas, N.A. Mechanisms of solute and drug transport in relaxing, swellable, hydrophilic glassy polymers. *Polymer* **1999**, *40*, 3383–3398. [CrossRef]

81. Hill, A.J.; Thornton, A.W.; Hannink, R.H.J.; Moon, J.D.; Freeman, B.D. Role of free volume in molecular mobility and performance of glassy polymers for corrosion-protective coatings. *Corros. Eng. Sci. Technol.* **2020**, *55*, 145–158. [CrossRef]

82. Vergara, J.H.; La Scala, J.J.; Henry, C.K.; Sadler, J.M.; Yadav, S.K.; Palmese, G.R. The effect of pendant alkyl chain length on the barrier properties of epoxy/amine crosslinked networks. *Polymer* **2017**, *132*, 133–142. [CrossRef]

83. Merachtsaki, D.; Xidas, P.; Giannakoudakis, P.; Triantafyllidis, K.; Spathis, P. Corrosion protection of steel by epoxy-organoclay nanocomposite coatings. *Coatings* **2017**, *7*, 84. [CrossRef]

84. Kostina, Z.I.; Krylova, S.A.; Ponurko, I.V. Production and properties of glassy metaphosphate composition for protecting the elements of water-heating systems from corrosion. *Glass Ceram.* **2016**, *73*, 71–74. [CrossRef]

85. Sharma, A.; Kumar, S.; Tripathi, B.; Singh, M.; Vijay, Y.K. Aligned CNT/Polymer nanocomposite membranes for hydrogen separation. *Int. J. Hydrog. Energy* **2009**, *34*, 3977–3982. [CrossRef]

86. Park, S.; Bang, J.; Choi, J.; Lee, S.H.; Lee, J.-H.; Lee, J.S. 3-Dimensionally disordered mesoporous silica (DMS)-containing mixed matrix membranes for CO_2 and non-CO_2 greenhouse gas separations. *Sep. Purif. Technol.* **2014**, *136*, 286–295. [CrossRef]

87. Kramer, P.W.; Murphy, M.K.; Stookey, D.J.; Henis, J.M.; Stedronsky, E.R. Membranes Having Enhanced Selectivity and Method of Producing Such Membranes. U.S. Patent 5,215,554, 1 June 1993.

88. Liu, C.; Karns, N.K.; Jan, D.Y. High Flux, Cross-Linked, Fumed Silica Reinforced Polyorganosiloxane Membranes for Separations. U.S. Patent 15,685,996, 17 May 2018.

89. Choi, S.H.; Al-Qahtani, M.S.; Qasem, E.A. Multilayer Aromatic Polyamide Thin-Film Composite Membranes for Separation of Gas Mixtures. U.S. Patent 10,682,606, 16 June 2020.

90. Salem, A.; Ghoreyshi, A.A. Modelling of water/organic vapor dehydration by glassy polymer membranes. *Desalination* **2006**, *193*, 25–34. [CrossRef]

91. Gomes, D.; Nunes, S.P.; Peinemann, K.-V. Membranes for gas separation based on poly(1-trimethylsilyl-1-propyne)–silica nanocomposites. *J. Membr. Sci.* **2005**, *246*, 13–25. [CrossRef]

92. Martin, M.; Hanagud, S.; Thadhani, N.N. Mechanical behavior of nickel+aluminum powder-reinforced epoxy composites. *Mater. Sci. Eng. A* **2007**, *443*, 209–218. [CrossRef]

93. Jordan, J.L.; Spowart, J.E.; Kendall, M.J.; Woodworth, B.; Siviour, C.R. Mechanics of particulate composites with glassy polymer binders in compression. *Philos. Trans. R. Soc. A Math. Phys. Eng. Sci.* **2014**, *372*, 20130215. [CrossRef] [PubMed]

94. Seo, J.; Kim, S.; Samal, S.; Kim, H. Viscous behaviour of Bi2O3–B2O3–ZnO glass composites with ceramic fillers. *Adv. Appl. Ceram.* **2014**, *113*, 334–340. [CrossRef]

95. Samal, S.; Kim, S.; Kim, H. Effects of Filler Size and Distribution on Viscous Behavior of Glass Composites. *J. Am. Ceram. Soc.* **2012**, *95*, 1595–1603. [CrossRef]

96. Shin, H.; Kim, S.-G.; Park, J.-S.; An, J.-S.; Hong, K.S.; Kim, H. Co-Additions of TiO2 and SiO2 Crystalline Fillers to Tailor the Properties of BaO–ZnO–B2O3–SiO2 Glass for Application to Barrier Ribs of Plasma Display Panels. *J. Am. Ceram. Soc.* **2006**, *89*, 3258–3261. [CrossRef]

97. Lin, C.W.; Huang, L.C.; Ma, C.C.M.; Yang, A.C.M.; Lin, C.J.; Lin, L.J. Nanoplastic flows of glassy polymer chains interacting with multiwalled carbon nanotubes in nanocomposites. *Macromolecules* **2008**, *41*, 4978–4988. [CrossRef]

98. Merkel, T.C.; Freeman, B.D.; Spontak, R.J.; He, Z.; Pinnau, I.; Meakin, P.; Hill, A.J. Ultrapermeable, reverse-selective nanocomposite membranes. *Science* **2002**, *296*, 519–522. [CrossRef] [PubMed]

99. Poslinski, A.J.; Ryan, M.E.; Gupta, R.K.; Seshadri, S.G.; Frechette, F.J. Rheological behavior of filled polymeric systems II. The effect of a bimodal size distribution of particulates. *J. Rheol.* **1988**, *32*, 751–771. [CrossRef]

100. Brouwers, H.J. Particle-size distribution and packing fraction of geometric random packings. *Phys. Rev. E Stat. Nonlinear Soft Matter Phys.* **2006**, *74*, 031309. [CrossRef] [PubMed]

101. Yang, W.; Yu, S.; Sun, R.; Du, R. Nano- and microsize effect of CCTO fillers on the dielectric behavior of CCTO/PVDF composites. *Acta Mater.* **2011**, *59*, 5593–5602. [CrossRef]

102. Asai, K.; Amao, Y.; Iijima, Y.; Okura, I.; Nishide, H. Novel Pressure-Sensitive Paint for Cryogenic and Unsteady Wind-Tunnel Testing. *J. Thermophys. Heat Transf.* **2002**, *16*, 109–115. [CrossRef]

103. Loui, A.; Ratto, T.V.; Wilson, T.S.; McCall, S.K.; Mukerjee, E.V.; Love, A.H.; Hart, B.R. Chemical vapor discrimination using a compact and low-power array of piezoresistive microcantilevers. *Analyst* **2008**, *133*, 608–615. [CrossRef]

104. Hubmann, M.; Kong, X.; Curtis, J.M. Kinetic stabilization of cellulose nanocrystals in a photocurable prepolymer for application as an adhesion promoter in UV-curable coatings. *Prog. Org. Coat.* **2019**, *129*, 101–115. [CrossRef]

105. Viard, A.; Gottardo, L.; Lopez-Ferber, D.; Soleilhavoup, A.; Salameh, C.; Samal, S.; Gueguen, Y.; Rouxel, T.; Motz, G.; Babonneau, F.; et al. Molecular design of melt-spinnable co-polymers as Si–B–C–N fiber precursors. *Dalton Trans.* **2017**, *46*, 13510–13523. [CrossRef]

106. Hutchinson, J.M. Physical aging of polymers. *Prog. Polym. Sci.* **1995**, *20*, 703–760. [CrossRef]

107. Cangialosi, D.; Boucher, V.M.; Alegría, A.; Colmenero, J. Physical aging in polymers and polymer nanocomposites: Recent results and open questions. *Soft Matter* **2013**, *9*, 8619–8630. [CrossRef]

108. Pfromm, P.H.; Koros, W.J. Accelerated physical ageing of thin glassy polymer films: Evidence from gas transport measurements. *Polymer* **1995**, *36*, 2379–2387. [CrossRef]

109. Jérôme, B.; Commandeur, J. Dynamics of glasses below the glass transition. *Nature* **1997**, *386*, 589–592. [CrossRef]

110. Chung, T.-S.; Khean Teoh, S. The ageing phenomenon of polyethersulphone hollow fibre membranes for gas separation and their characteristics. *J. Membr. Sci.* **1999**, *152*, 175–188. [CrossRef]

111. McCaig, M.S.; Paul, D.R. Effect of film thickness on the changes in gas permeability of a glassy polyarylate due to physical aging Part I. Experimental observations. *Polymer* **2000**, *41*, 629–637. [CrossRef]

112. Kim, J.H.; Koros, W.; Paul, D.R. Effects of CO2 exposure and physical aging on the gas permeability of thin 6FDA-based polyimide membranes: Part 2. With crosslinking. *J. Membr. Sci.* **2006**, *282*, 32–43. [CrossRef]

113. Struik, L.C.E. Volume relaxation in polymers. *Rheol. Acta* **1966**, *5*, 303–311. [CrossRef]

114. Xia, J.; Chung, T.-S.; Paul, D.R. Physical aging and carbon dioxide plasticization of thin polyimide films in mixed gas permeation. *J. Membr. Sci.* **2014**, *450*, 457–468. [CrossRef]

115. Xia, J.; Chung, T.-S.; Li, P.; Horn, N.R.; Paul, D.R. Aging and carbon dioxide plasticization of thin polyetherimide films. *Polymer* **2012**, *53*, 2099–2108. [CrossRef]

116. Tiwari, R.R.; Jin, J.; Freeman, B.D.; Paul, D.R. Physical aging, CO2 sorption and plasticization in thin films of polymer with intrinsic microporosity (PIM-1). *J. Membr. Sci.* **2017**, *537*, 362–371. [CrossRef]

117. Huang, Y.; Paul, D.R. Physical Aging of Thin Glassy Polymer Films Monitored by Optical Properties. *Macromolecules* **2006**, *39*, 1554–1559. [CrossRef]

118. Drozdov, A.D. The effect of temperature on physical aging of glassy polymers. *J. Appl. Polym. Sci.* **2001**, *81*, 3309–3320. [CrossRef]

119. Yong, W.F.; Kwek, K.H.A.; Liao, K.-S.; Chung, T.-S. Suppression of aging and plasticization in highly permeable polymers. *Polymer* **2015**, *77*, 377–386. [CrossRef]